
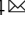


# Alt-RPL36 downregulates the PI3K-AKT-mTOR signaling pathway by interacting with TMEM24

Xiongwen Cao<sup>1,2,5</sup>, Alexandra Khitun<sup>1,2,5</sup>, Yang Luo<sup>1,2</sup>, Zhenkun Na<sup>1,2</sup>, Thitima Phoodokmai<sup>3</sup>, Khomkrit Sappakhaw<sup>3</sup>, Elizabeth Olatunji<sup>2</sup>, Chayasith Uttamapinant<sup>3</sup> & Sarah A. Slavoff<sup>1,2,4</sup>  

Thousands of human small and alternative open reading frames (smORFs and alt-ORFs, respectively) have recently been annotated. Many alt-ORFs are co-encoded with canonical proteins in multicistronic configurations, but few of their functions are known. Here, we report the detection of alt-RPL36, a protein co-encoded with human RPL36. Alt-RPL36 partially localizes to the endoplasmic reticulum, where it interacts with TMEM24, which transports the phosphatidylinositol 4,5-bisphosphate (PI(4,5)P<sub>2</sub>) precursor phosphatidylinositol from the endoplasmic reticulum to the plasma membrane. Knock-out of alt-RPL36 increases plasma membrane PI(4,5)P<sub>2</sub> levels, upregulates PI3K-AKT-mTOR signaling, and increases cell size. Alt-RPL36 contains four phosphoserine residues, point mutations of which abolish interaction with TMEM24 and, consequently, alt-RPL36 effects on PI3K signaling and cell size. These results implicate alt-RPL36 as an upstream regulator of PI3K-AKT-mTOR signaling. More broadly, the *RPL36* transcript encodes two sequence-independent polypeptides that co-regulate translation via different molecular mechanisms, expanding our knowledge of multicistronic human gene functions.

<sup>1</sup>Department of Chemistry, Yale University, New Haven, CT 06520, USA. <sup>2</sup>Chemical Biology Institute, Yale University, West Haven, CT 06516, USA.

<sup>3</sup>School of Biomolecular Science and Engineering, Vidyasirimedhi Institute of Science and Technology (VISTEC), Rayong, Thailand. <sup>4</sup>Department of Molecular Biophysics and Biochemistry, Yale University, New Haven, CT 06529, USA. <sup>5</sup>These authors contributed equally: Xiongwen Cao, Alexandra Khitun.

✉email: [sarah.slavoff@yale.edu](mailto:sarah.slavoff@yale.edu)

Thousands of previously unannotated small and alternative open reading frames (smORFs, <100 amino acids, and alt-ORFs, >100 amino acids, respectively) have recently been revealed via genomic and proteomic technologies in mammalian genomes<sup>1,2</sup>. These genes previously escaped annotation not just because of their short length, but because, as a class, they exhibit low homology to proteins of known function, and are enriched for initiation at near-cognate non-AUG start codons (~50%)<sup>3,4</sup>. Interestingly, while many smORFs and alt-ORFs lie in regions of RNA previously annotated as non-coding, up to 30% of the alt-ORFs identified by LC-MS/MS overlap an annotated protein-coding sequence in a different reading frame<sup>2</sup>. A rapidly increasing number of smORFs and alt-ORFs have been shown to play important roles in mammalian biology<sup>5,6</sup>. For example, NBDY regulates the mRNA decapping complex in human cells<sup>7</sup>, PIGBOS regulates the endoplasmic reticulum (ER) stress response<sup>8</sup>, and the MIEF1 microprotein regulates mitochondrial protein translation<sup>9</sup>. In mouse, AW112010 is a required component of the innate immune response<sup>10</sup>, and myoregulin interacts with SERCA calcium channels in muscle<sup>11</sup>. Recently, a genome-scale CRISPR screen revealed that over 500 smORFs regulate growth of human induced pluripotent stem cells<sup>12</sup>. These findings demonstrate that assignment of functions to small proteins represents a major opportunity to gain insights into biology.

Currently, there is proteomic evidence for hundreds of uncharacterized human smORFs and alt-ORFs that are co-encoded with annotated proteins and initiate at non-AUG start codons. These findings are, in many cases, supported by ribosome profiling, conservation analyses, and in silico prediction of functional domains and secondary structure<sup>13–15</sup>. However, a majority of multicistronic and/or non-AUG-initiated alt-ORFs remain biochemically uncharacterized. Notable exceptions include the MIEF1 microprotein, which is encoded in a 5'UTR and regulates translation by mitoribosomes<sup>9</sup>, and Aw112010, which initiates at a near-cognate start codon and is required for mucosal immunity<sup>10</sup>.

Multiple human ribosomal proteins are encoded in complex genes that co-express two independent functional proteins. For example, ribosomal proteins L40 and S27A are synthesized as preproteins fused to ubiquitin, and S30 as a fusion to ubiquitin-like protein<sup>16</sup>. A prior proteogenomics study revealed translation of a sequence-independent alt-ORF co-encoded with human 60S ribosomal protein L36 (RPL36)<sup>17</sup>, which has nonetheless remained unannotated, likely due to a lack of information about its start codon and function.

TMEM24 (transmembrane protein 24; alternatively C2CD2L, C2 domain-containing protein 2-like) is an endoplasmic reticulum (ER)-anchored membrane protein that mediates ER-plasma membrane (PM) contacts, transporting the PI(4,5)P<sub>2</sub> precursor phosphatidylinositol from the ER to the PM<sup>18</sup>. This activity is required to replenish PI(4,5)P<sub>2</sub> after its phosphorylation by phosphoinositide 3-kinase (PI3K) enzymes to generate phosphatidylinositol-3,4,5-trisphosphate (PI(3,4,5)P<sub>3</sub>) and downstream signaling lipids<sup>19</sup>, which activate the AKT-mTOR pathway to control cell growth and protein synthesis<sup>20,21</sup>. The localization of TMEM24 to ER-PM contacts is regulated by dynamic phosphorylation of the C-terminal region of TMEM24. Ca<sup>2+</sup>-stimulated phosphorylation causes TMEM24 dissociation from the PM, and dephosphorylation allows TMEM24 to re-associate with the PM<sup>18</sup>. TMEM24 is highly expressed in the brain and pancreatic islets<sup>22</sup>, and loss of TMEM24 in insulin-secreting cells leads to a defect in insulin release<sup>18,23</sup>.

In this study, we provide molecular and proteomic evidence for the existence of an alternative protein co-encoded with human RPL36, which we term alt-RPL36. We demonstrate that alt-RPL36 translation initiates from an upstream non-AUG start

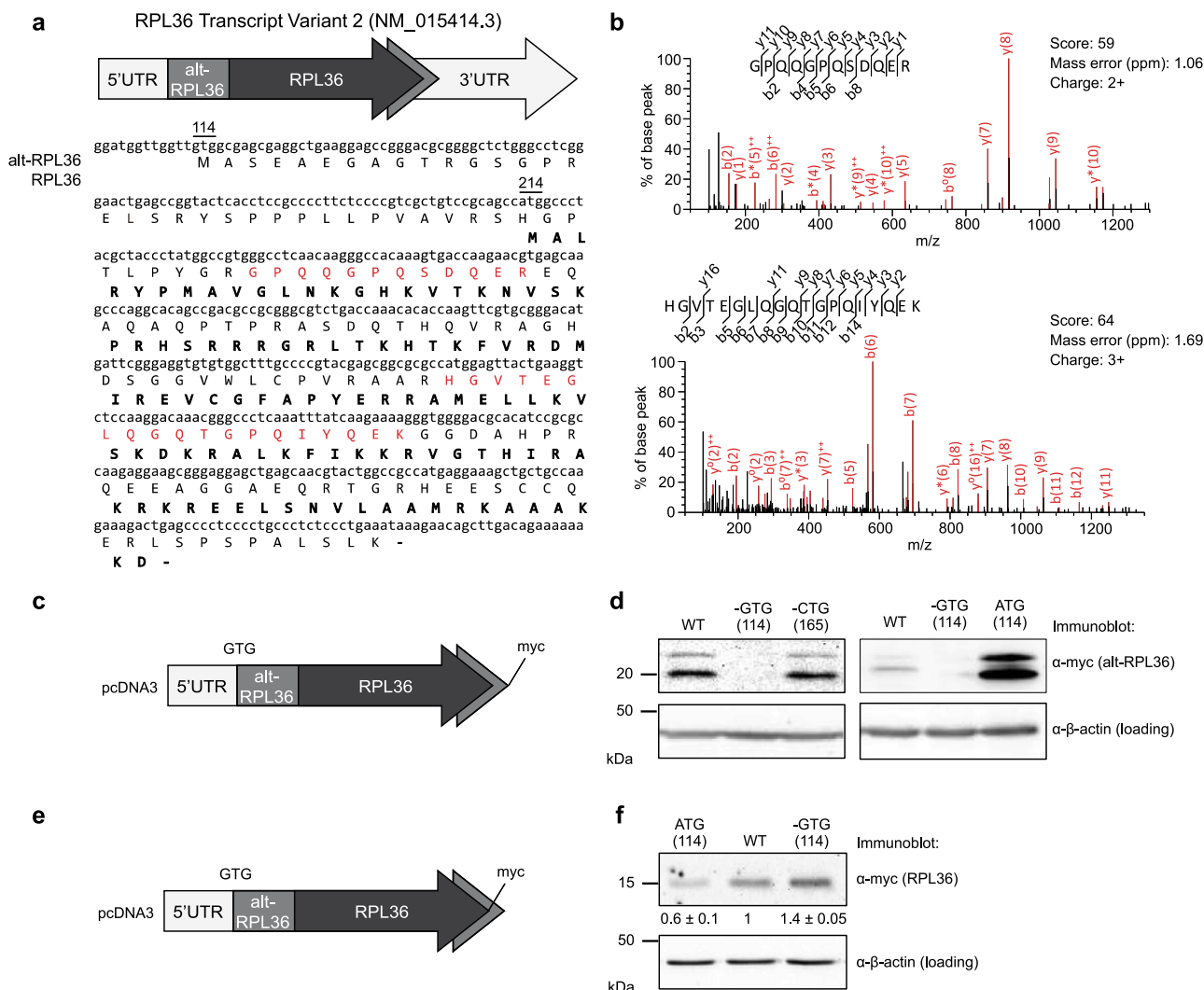
codon in human RPL36 transcript variant 2. We show that alt-RPL36 partially localizes to the ER in human cells using genomic knock-in tagging and unnatural amino acid labeling. We identify and map four phosphorylation sites that are present at high stoichiometry in alt-RPL36, and show that phosphorylation is required for interaction with TMEM24. Finally, we engineer specific alt-RPL36 knockout and rescue cell lines to demonstrate that loss of alt-RPL36 increases TMEM24-dependent plasma membrane PI(4,5)P<sub>2</sub> levels, activates the PI3K-AKT-mTOR pathway and increases cell size. These results implicate alt-RPL36 as an upstream regulator of phospholipid transport and PI3K-AKT-mTOR signaling and demonstrate that overlapping ORFs in the RPL36 gene encode proteins that play related, but mechanistically distinct, biological roles in *trans*.

## Results

**A GUG-initiated alternative protein is translated from RPL36 transcript variant 2.** Using a previously reported proteogenomic strategy for unannotated small protein discovery<sup>2</sup>, we identified two tryptic peptides that mapped uniquely to an alternative reading frame of human RPL36 transcript variant 2 in HEK 293T cells, which encodes an alternative protein we name alt-RPL36 (Fig. 1a, b, and Supplementary Data 1). One of these tryptic fragments was also previously identified in the supplementary information of a proteogenomic study of A431 cells but was not characterized<sup>17</sup>. One alt-RPL36 tryptic peptide was also detected in HT1080 and MOLT4 cells (Supplementary Fig. 1a, b, and Supplementary Data 1), consistent with expression in several human cell lines from different tissues of origin. Compared to transcript variant 1 (NCBI RefSeq NM\_033643), RPL36 variant 2 (NCBI RefSeq NM\_015414 and Fig. 1a) contains a longer 5'UTR, which we hypothesized to contain a start codon initiating alt-RPL36 translation. Interestingly, the first stop codon in-frame with the observed tryptic peptides is downstream of the RPL36 stop codon, meaning that alt-RPL36 is longer than RPL36 and completely encompasses its coding sequence. However, since alt-RPL36 is translated in the -1 reading frame relative to RPL36, the amino acid sequences of these two proteins are completely different (Fig. 1a).

To confirm translation and identify the start codon of alt-RPL36, the cDNA sequence comprising the 5'UTR of RPL36 transcript variant 2 through the stop codon of the putative alt-ORF was cloned into a mammalian expression vector with a myc tag appended to the 3' end of alt-RPL36. This construct produces two anti-myc immunoreactive bands (~22 and ~20 kDa apparent molecular weight, due to phosphorylation, *vide infra*) from the alt-RPL36 reading frame when transiently transfected into HEK 293T cells (Fig. 1d, lanes 1 and 4). Because there is no upstream AUG start codon in-frame with the observed alt-RPL36 tryptic peptides, we hypothesized that alt-RPL36 initiates at a near-cognate start codon, which can initiate protein translation with methionine at a fractional efficiency relative to AUG<sup>24,25</sup>. We searched the upstream, in-frame DNA sequence of alt-RPL36, and found two possible near-cognate start codons in a strong Kozak sequence context: G<sub>114</sub>TG and C<sub>165</sub>TG (numbered relative to the first nucleotide of the cDNA). Deletion of G<sub>114</sub>TG, but not C<sub>165</sub>TG, abolished the expression of alt-RPL36 (Fig. 1d, lanes 2, 3, and 5), and mutation of G<sub>114</sub>TG to A<sub>114</sub>TG increased the expression of alt-RPL36, consistent with increased efficiency of initiation at AUG codons<sup>26</sup> (Fig. 1d, lane 6), indicating that G<sub>114</sub>TG is the start of the alt-RPL36 coding sequence.

Epitope-tagging of the RPL36 coding sequence revealed that the annotated ribosomal protein is also translated from RPL36 transcript variant 2, and that translation of alt-RPL36 has a small (~40%) inhibitory effect on RPL36 synthesis from transcript



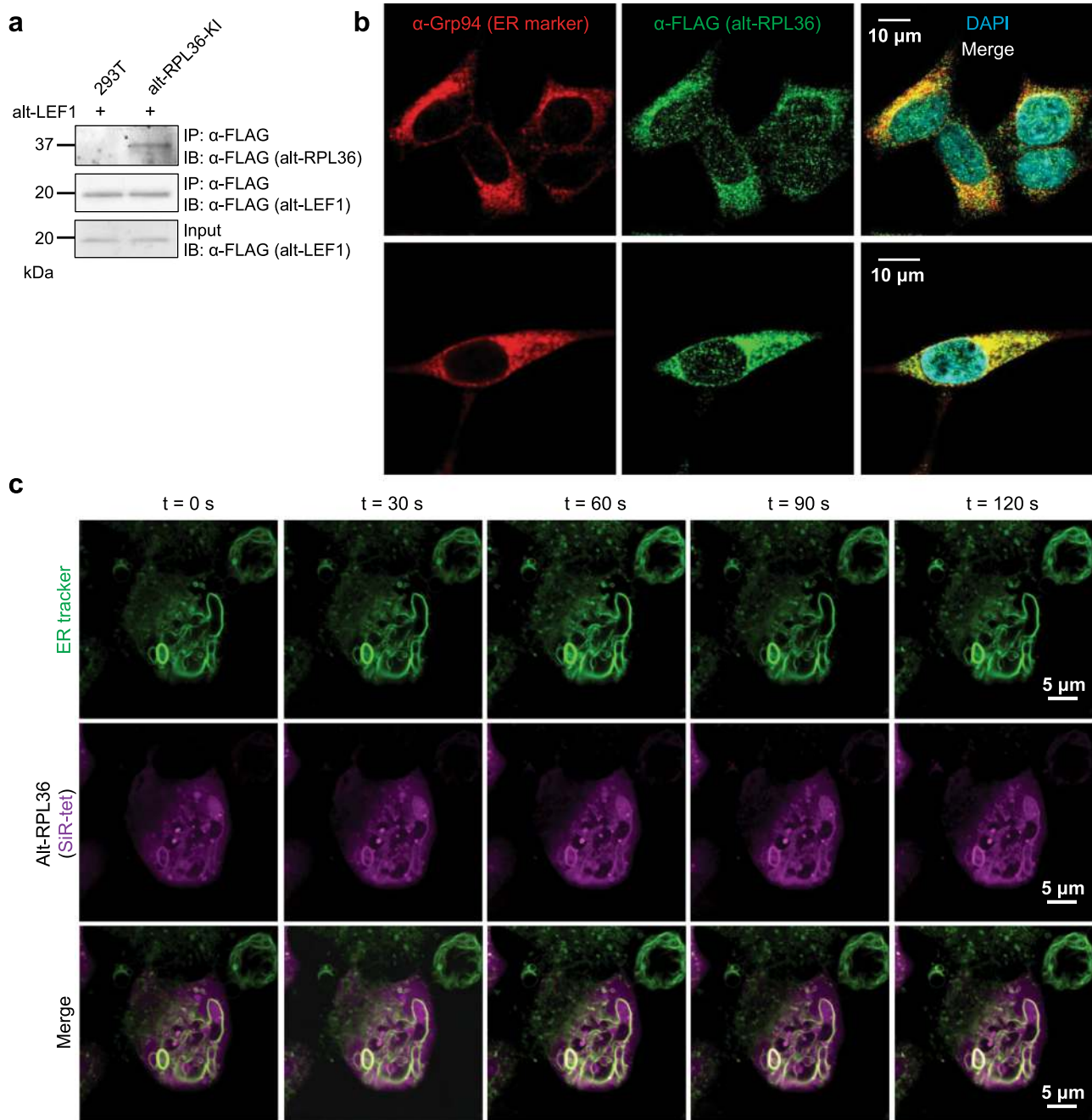
**Fig. 1 A GUG-initiated alternative protein is translated from RPL36 transcript variant 2.** **a** Top: a schematic representation of human RPL36 transcript variant 2 (tv 2); light gray arrow, 5' and 3' untranslated regions (UTR); mid gray, alternative open reading frame (alt-ORF) encoding alt-RPL36; dark gray, annotated RPL36 coding sequence. Bottom: the cDNA sequence of human RPL36 transcript variant 2 is shown with the protein sequences of alt-RPL36 and RPL36 (bold) indicated below. The GTG start codon of alt-RPL36 and ATG start codon of RPL36 are numbered above the cDNA sequence. Highlighted in red are two tryptic peptides of alt-RPL36 detected by LC-MS/MS. **b** MS/MS spectra of two alt-RPL36 tryptic peptides detected via peptidomics in HEK 293T cells. **c, d** Expression of a construct containing the full 5'UTR and alt-RPL36 coding sequence derived from RPL36 tv 2, with a myc tag appended to the C-terminus of alt-RPL36 (**c**), in HEK 293T cells, was followed by lysis and western blotting with the antibodies indicated to the right (**d**). **e, f** Expression of a construct containing the full 5'UTR and alt-RPL36 coding sequence derived from RPL36 tv 2, with a myc tag appended to the C-terminus of RPL36 (**e**), in HEK 293T cells, was followed by lysis and western blotting with the antibodies indicated to the right (**f**). Quantitative analysis of the western blot signal of RPL36-myc are indicated at the bottom. Data represent mean values ± standard error of the mean (s.e.m.) of three biological replicates. Source data are provided as a Source data file. All western blots are representative of results obtained in three biological replicates.

variant 2. This is consistent with co-regulated expression of both ORFs from this transcript, as previously reported for uORFs initiating at non-AUG start codons<sup>26</sup> (Fig. 1e, f). Taken together, these results indicate that human RPL36 transcript variant 2 generates both RPL36 and an alternative protein, alt-RPL36, that initiates from G<sub>114</sub>TG, in overlapping reading frames.

To determine whether alt-RPL36 is conserved among species, RPL36 mRNAs from different species were obtained from NCBI nucleotide database, then translated in the +1, +2, and +3 frames using the ExPaSy translate tool. Cognate or near-cognate start codons within Kozak consensus motifs in-frame with sequences homologous to human alt-RPL36 were identified in the 5'UTR of each transcript in order to predict the full-length sequence of hypothetical alt-RPL36 homologs. ClustalW alignment of hypothetical alt-RPL36 homologs from cat, cattle, and

monkey revealed significant sequence similarity (Supplementary Fig. 2c), though protein-level experimental evidence for these hypothetical homologs does not currently exist.

**Endogenously expressed alt-RPL36 partially localizes to the endoplasmic reticulum.** Next, we wanted to determine whether alt-RPL36 is endogenously expressed from the RPL36 genomic locus. To this end, we generated a knock-in (KI) HEK 293T cell line with a 3xGFP11-FLAG tag appended to the 3' end of alt-RPL36. FLAG-IP followed by western blotting revealed that the KI cells produced two specific anti-FLAG immunoreactive bands with the expected molecular weights, one major lower-mobility band and one faint higher mobility band, which were consistent with the overexpression results and which were absent in control



**Fig. 2** Alt-RPL36 is endogenously expressed and partially localizes to the endoplasmic reticulum. **a** Control HEK 293T cells (lane 1) or alt-RPL36-GFP11-FLAG knock-in (KI) HEK 293T cells (lane 2) were transfected with alt-LEF1-FLAG (which is a recently identified ~20 kDa alt-ORF[1]), serving as a FLAG-IP control, and IPs were performed with anti-FLAG antibody followed by IB with anti-FLAG. Cell lysates (1%) before IP (input) were used as the loading controls. Data are representative of three biological replicates. **b** Confocal imaging of alt-RPL36-GFP11-FLAG KI cells after immunostaining with anti-Grp94 (red), anti-FLAG (green), and DAPI (cyan). Scale bar, 10  $\mu$ m. Data are representative of three biological replicates. **c** Live-cell imaging of alt-RPL36 via genetic code expansion. HEK 293T cells were transfected with plasmids expressing *M. mazei* pyrrolysyl-tRNA synthetase bearing Y306A/Y384F mutations (PylRS-AF), amber-suppressing Pyl tRNA (PylT<sub>CUA</sub>), and alt-RPL36<sup>L18TAG</sup>. Cells were incubated with 60  $\mu$ M bicyclononyne-lysine (BCNK) for 45 h, then labeled with tetrazine-silicon rhodamine (SiR-tet, magenta) and a live-cell ER tracker DPX dye (green) for 30 min before live-cell imaging. Time-lapse imaging over 2 min was shown. Scale bar, 5  $\mu$ m. Data are representative of three biological replicates.

HEK 293T cells, indicating the endogenous expression of alt-RPL36 (Fig. 2a).

To further confirm the endogenous expression and investigate the subcellular localization of alt-RPL36, we performed immunostaining with the KI cells. As shown in Fig. 2b, endogenously expressed alt-RPL36-3xGFP11-FLAG partially co-localizes with

Grp94, an ER marker, indicating that a subset of alt-RPL36 localizes to ER.

To further confirm the subcellular localization of alt-RPL36, we visualized dynamics of alt-RPL36 in living cells via genetic code expansion-mediated labeling. A single amino acid residue of alt-RPL36 was replaced with a bicyclononyne-lysine (BCNK)

unnatural amino acid via an engineered amber-suppressor pyrrolysyl tRNA (Pyl tRNA<sub>CUA</sub>/Pyl tRNA synthetase (PylRS) pair<sup>27</sup>. Alt-RPL36 bearing BCNK is subsequently derivatized with a membrane-permeable tetrazine-silicon rhodamine (SiR) conjugate via inverse-electron-demand Diels-Alder reaction for visualization in live cells<sup>27</sup>. We identified one amber variant—alt-RPL36<sup>L18TAG</sup>—which showed BCNK-dependent expression to produce full-length alt-RPL36 (Supplementary Fig. 3), and could be labeled in live HEK 293T cells with tetrazine-SiR. SiR-labeled alt-RPL36<sup>L18BCNK</sup> was primarily cytosolic—which could be an artefact of overexpression under genetic code expansion—but a subpopulation of the protein showed clear overlap with ER tubules (Fig. 2c), suggesting ER localization of alt-RPL36. Taken together, these results indicate that alt-RPL36 is endogenously expressed and partially localizes to the ER.

**Four serine residues of alt-RPL36 are phosphorylated.** To test whether alt-RPL36 exhibits two bands by western blot analysis (Fig. 1d, lane 1) due to protein phosphorylation<sup>28</sup>, alt-RPL36 was immunopurified from HEK 293T cells stably expressing alt-RPL36-FLAG-HA and treated with a nonspecific phosphatase. Phosphatase treatment eliminated the upper band, suggesting that it represents a phosphorylated form of alt-RPL36 (Fig. 3a). To identify the phosphorylated residues, we performed LC-MS/MS with immunopurified, digested alt-RPL36, and identified four candidate phosphoserine residues (S19, S22, S140, and S142) (Fig. 3b, Supplementary Data 2).

Because no phosphoantibodies specific to alt-RPL36 yet exist, we employed Phos-tag SDS-PAGE and western blotting, combined with mutational analysis, to confirm the phosphorylation sites identified by LC-MS/MS. As shown in Fig. 3c (lane 2), alt-RPL36 exhibited four bands corresponding to constitutively phosphorylated variants. Only the bottom band remained after nonspecific phosphatase treatment, indicating that it represents unphosphorylated alt-RPL36 (Fig. 3c, lane 1). Mutation of S19 to alanine abolished the second band, and mutation of S22 to alanine eliminated both the first and the second bands (Fig. 3c, lanes 3 and 4), suggesting that the second band represents pS19, the first band is pS22, and pS22 is required for phosphorylation of S19. Single mutation of S140 or S142 to alanine attenuated the signal of the third band (Fig. 3c, lanes 5 and 6), and double mutation of S140 and S142 to alanine abolished the third band entirely (Fig. 3c, lane 7), suggesting the third band represents both S140 and S142-phosphorylated alt-RPL36. The quadruple mutant S19A S20A S140A S142A exhibited a single band comigrating with phosphatase-treated wild-type alt-RPL36, further confirming that these four serine residues are the phosphorylation sites. Quantitation of replicate western blots revealed that ~86% of alt-RPL36 is constitutively phosphorylated (Fig. 3d). High-occupancy phosphorylation of four specific sites in alt-RPL36 is consistent with a functional role for the protein.

**Phosphorylated alt-RPL36 interacts with TMEM24 via the SMP and C2 domains.** Because many small proteins characterized to date bind to and regulate other proteins<sup>29</sup>, we performed a two-step co-immunoprecipitation (co-IP) of dually FLAG- and HA-tagged alt-RPL36 from HEK 293T cells and identified proteins specifically enriched over untransfected controls via quantitative proteomics. We then excluded common contaminants and proteins nonspecifically enriched by other previously reported, intrinsically disordered microproteins<sup>7,30–32</sup>. This analysis revealed that phospholipid transfer protein TMEM24/C2CD2L specifically co-immunopurifies with alt-RPL36 (Fig. 4a, Supplementary Data 3). To confirm the LC-MS/MS results, we performed reciprocal co-IP and western blotting and observed

enrichment of overexpressed alt-RPL36-myc by TMEM24-FLAG over controls (Fig. 4b, c).

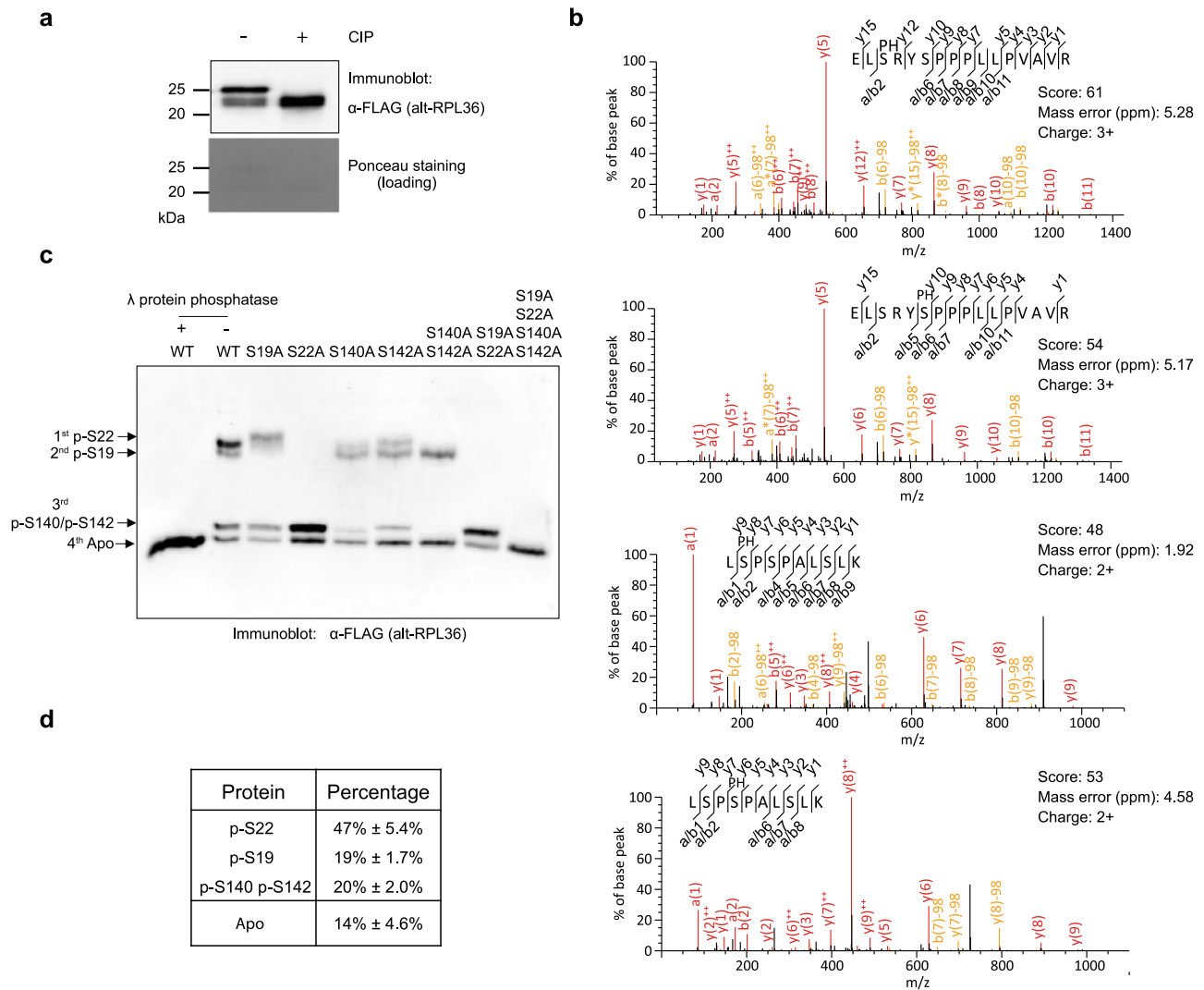
TMEM24 consists of an N-terminal transmembrane domain that resides in the ER membrane, an SMP domain, a C2 domain, and an unstructured C-terminal region that interacts with the plasma membrane (Fig. 4d)<sup>18</sup>. To determine the domain(s) of TMEM24 with which alt-RPL36 interacts, we generated a series of truncation mutants of TMEM24 (Fig. 4d), transiently transfected these constructs into HEK 293T cells stably expressing alt-RPL36-FLAG-HA, and examined their ability to interact with alt-RPL36 by co-IP and western blotting. Deletion of the N-terminal or the C-terminal regions of TMEM24 maintained the interaction (Fig. 4e, f), while further deletion of either the C2 domain or the SMP domain abolished the interaction (Supplementary Fig. 4a, b), indicating that both SMP and C2 domains are required for the interaction with alt-RPL36.

Since alt-RPL36 is constitutively phosphorylated, we asked whether these modifications regulate its interaction with TMEM24. As shown in Fig. 4g, while wild-type, phosphorylated alt-RPL36 interacts with TMEM24, the quadruple alanine mutant, which abolishes all phosphorylation of alt-RPL36, eliminates the interaction. This may be due to reduction of the binding affinity to TMEM24 or change of the subcellular localization of alt-RPL36. These results indicate that the interaction between alt-RPL36 and the SMP and C2 domains of TMEM24 is specific and requires phosphorylation of alt-RPL36.

To determine whether endogenously expressed alt-RPL36 co-localizes with TMEM24 in cells, we transiently transfected TMEM24-GFP into alt-RPL36-FLAG KI cells, followed by immunostaining. As shown in Fig. 4h, endogenous alt-RPL36 co-localizes with overexpressed TMEM24, consistent with an interaction between these proteins in cells. The plasma membrane localization of both TMEM24-GFP and alt-RPL36-FLAG in this experiment may be due to increased ER-plasma membrane junction formation upon TMEM24 overexpression, as previously reported<sup>22</sup>. To determine whether TMEM24 is required for the ER localization of endogenous alt-RPL36, we knocked down TMEM24 with shRNA in the KI cells (Supplementary Fig. 5a, b), followed by immunostaining. As shown in Fig. 4i, j, TMEM24 knockdown reduced the correlation coefficient between ER marker Grp94 and alt-RPL36, suggesting that interaction with TMEM24 is required for the ER localization of alt-RPL36.

We hypothesized that, since alt-RPL36 likely exists in complex with TMEM24 in cells, the same kinase may recognize and phosphorylate both proteins. The C-terminal region of TMEM24 has been reported to be phosphorylated by protein kinase C (PKC)<sup>18</sup>. Treatment of purified recombinant alt-RPL36 with PKC led to generation of lower-migration phosphorylated species in a Phos-tag western blot (Supplementary Fig. 6a), indicating that PKC can phosphorylate alt-RPL36 in vitro. To determine whether PKC regulates the phosphorylation of alt-RPL36 in cells, we treated the HEK 293T cells stably expressing alt-RPL36-FLAG-HA with PKC inhibitor Bisindolylmaleimide II<sup>33</sup>, followed by FLAG-IP and Phos-tag western blot. As shown in Supplementary Fig. 6b, c, treatment with PKC inhibitor partially changes the phosphorylation pattern of alt-RPL36 in a dose-dependent manner, indicating PKC may, directly or indirectly, partially contribute to regulation of alt-RPL36 phosphorylation in cells.

It has been reported that phosphorylation of TMEM24 is regulated by the cytosolic calcium level<sup>18</sup>. We therefore asked whether the phosphorylation of alt-RPL36 is also dynamically regulated by changes in cytosolic calcium. To this end, we treated HEK 293T cells stably expressing alt-RPL36-FLAG-HA with thapsigargin, which elevates cytosolic calcium levels by blocking the ER calcium pump (SERCA)<sup>34</sup>, then measured phosphorylation of alt-RPL36 via Phos-tag western blot. As shown in



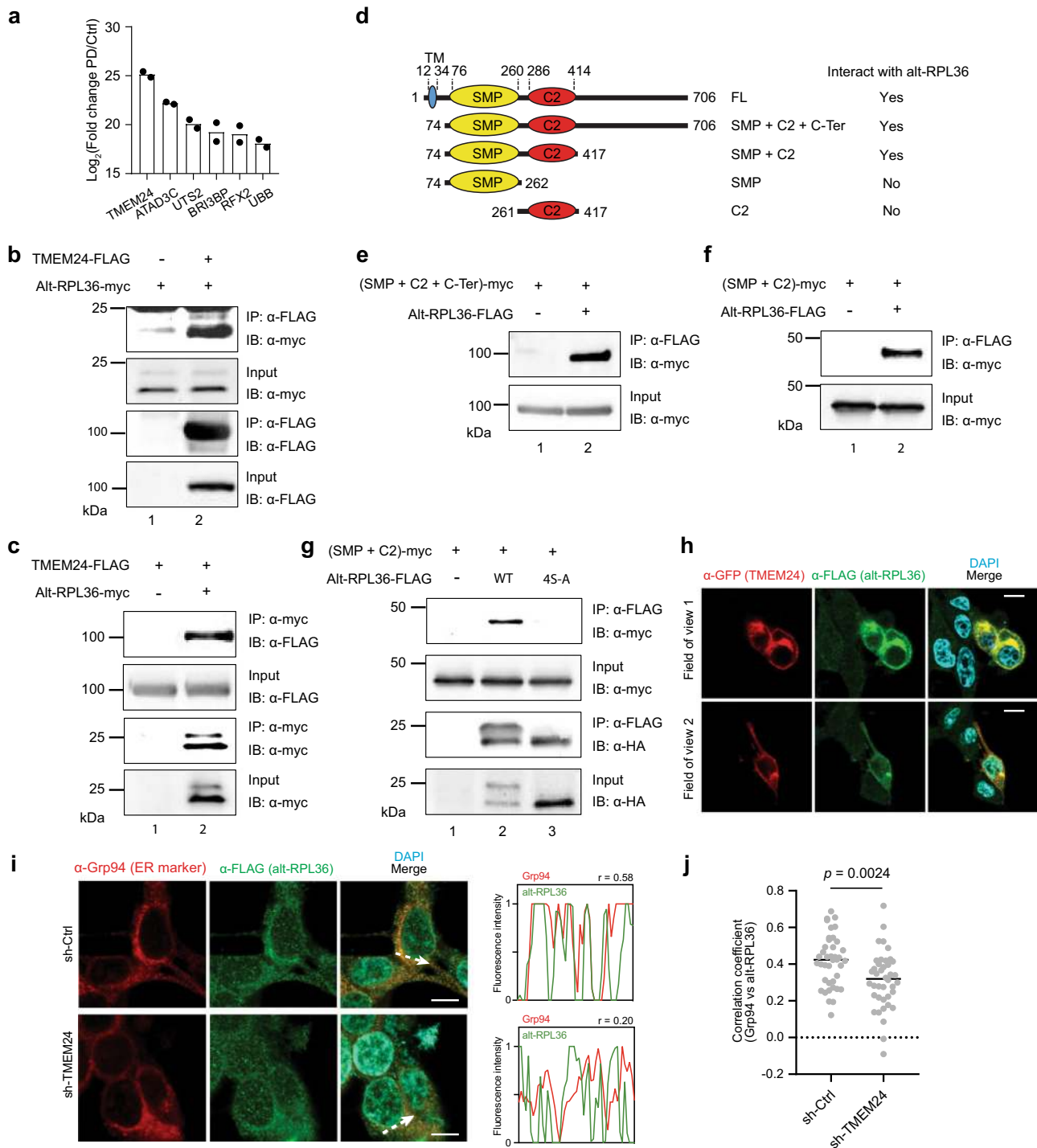
**Fig. 3 Four serine residues of alt-RPL36 are phosphorylated.** **a** Western blot analysis of immunoprecipitated alt-RPL36-FLAG-HA protein treated with calf intestinal alkaline phosphatase (CIP) and untreated control run on an SDS-PAGE gel. Ponceau staining served as a loading control. Data are representative of three biological replicates. **b** MS/MS spectra of alt-RPL36 phosphopeptides. S(PH) denotes phosphoserine. See Supplementary Data 2 for complete phosphoproteomics data. **c** To confirm phosphoserine assignments from MS/MS, wild-type alt-RPL36-FLAG, or alanine point mutants, were immunopurified from HEK 293T cells, resolved with Phos-tag SDS-PAGE, and detected with anti-FLAG antibody via western blot. A sample of wild-type alt-RPL36-FLAG was treated with  $\lambda$  protein phosphatase before Phos-tag SDS-PAGE (lane 1). Data are representative of three biological replicates. **d** Quantitative analysis of the western blot signal of wild-type alt-RPL36-FLAG. Data represent mean values  $\pm$  standard error of the mean (s.e.m.) of three biological replicates. Source data are provided as a Source data file.

Supplementary Fig. 6d, e, the phosphorylation pattern of alt-RPL36 changed within 15 min of thapsigargin treatment, indicating that phosphorylation of alt-RPL36 is dynamically regulated by cytosolic calcium.

**Phosphorylated alt-RPL36 regulates PI(4,5)P<sub>2</sub> transport and the PI3K–AKT–mTOR pathway.** TMEM24 is an ER-anchored membrane protein that transports phosphatidylinositol to the plasma membrane (PM) at ER-PM contact sites via its SMP domain<sup>18</sup>. Phosphatidylinositol is the precursor to PI(4,5)P<sub>2</sub>, which is converted by PI3K to PI(3,4,5)P<sub>3</sub> to regulate downstream AKT and mTOR signaling pathways<sup>19–21</sup>. To determine whether alt-RPL36 regulates TMEM24-dependent phenotypes, we generated an alt-RPL36-specific knockout (KO) HEK 293T cell line using CRISPR-Cas9. The CRISPR/Cas9 strategy targeted 210 nucleotides surrounding the alt-RPL36 start codon without perturbing the RPL36 coding sequence (Supplementary Fig. 7a).

Expression of the transcript variant 2-specific exon containing the alt-RPL36 start codon was undetectable via mRNA-seq and qRT-PCR in KO cells, but detectable in wild-type HEK 293T cells (Supplementary Fig. 7a, b). In the KO cells, expression of RPL36 was unchanged at the protein level, as indicated by western blotting, demonstrating that specific deletion of the alt-RPL36 start codon did not affect the total RPL36 protein level (Supplementary Fig. 7c). To determine that any observed phenotypic effects are specific to alt-RPL36 ablation in the KO, and not off-target effects, we also generated a “rescue” cell line in which the alt-RPL36 coding sequence was stably reintroduced on the KO background, as well as “4S-A rescue” cells, in which the non-phosphorylatable mutant of alt-RPL36 was reintroduced on the KO background.

We hypothesized that the effect of alt-RPL36 on TMEM24-dependent phosphatidylinositol transport could have outcomes at multiple levels: (1) PI(4,5)P<sub>2</sub> production in the plasma membrane immediately downstream of phosphatidylinositol transport, (2)



AKT-mTOR activation downstream of PI(4,5)P<sub>2</sub> phosphorylation by PI3K, and (3) transcriptional outputs downstream of AKT-mTOR pathway activation. Finally, phenotypic consequences should be exerted on cell morphology and size, which are regulated by PI3K and mTOR<sup>35,36</sup>. First, we assayed PI(4,5)P<sub>2</sub> levels at the plasma membrane in wild-type, alt-RPL36 knockout, rescue, and 4S-A rescue HEK 293T cell lines stably expressing PH-PLC-GFP, which is a PI(4,5)P<sub>2</sub> sensor<sup>37</sup>. As shown in Fig. 5a–c, knockout of alt-RPL36 increased the PH-PLC-GFP signal intensity compared with wild-type HEK 293T. The increase can be rescued by reintroduction of the coding sequence of wild-type, but not phosphorylation-incompetent, alt-RPL36. These results suggest that phosphorylated alt-RPL36 inhibits TMEM24-

dependent phosphatidylinositol transport, therefore inhibiting production of PI(4,5)P<sub>2</sub>.

To determine whether alt-RPL36 regulates the AKT-mTOR signaling pathway, we measured phosphorylation of these kinases and their substrates TSC2, S6K1, and S6, which correlates with pathway activation<sup>20,21</sup>. As demonstrated in Fig. 5d, knockout of alt-RPL36 increased the phosphorylation of AKT, TSC2, mTOR, S6K1, and S6. Furthermore, this effect can be rescued by reintroduction of wild-type, but not phosphorylation-incompetent, alt-RPL36, consistent with the PI(4,5)P<sub>2</sub> assay results. Interestingly, inhibition of mTOR by Torin1 reduced nascent alt-RPL36 translation, suggesting that mTOR regulates the translation of alt-RPL36 (Supplementary Fig. 8).

**Fig. 4 Phosphorylated alt-RPL36 interacts with TMEM24 via the SMP and C2 domains.** **a** Quantitative proteomics ( $N = 2$ ) of alt-RPL36-FLAG-HA pulldown (PD) from HEK 293T lysates identified putative alt-RPL36 interaction partners enriched over untransfected HEK 293T cells (Ctrl). Shown is the mean value of two biological replicates. For complete quantitative proteomics results, see Supplementary Data 3. **b, c** HEK 293T cells were transfected with alt-RPL36-myc only (**b**, lane 1), TMEM24-FLAG only (**c**, lane 1) or both plasmids (**b** and **c**, lane 2), and immunoprecipitation (IP) was performed with anti-FLAG (**b**) or anti-myc (**c**) antibody, followed by immunoblotting (IB) with antibodies indicated on the right. Cell lysates (1%) before IP (input) were used as the loading controls. **d** Schematic representation of the domain structures of the wild-type and truncation mutants of TMEM24, with amino acid residue numbers above. Alt-RPL36 interaction status of each construct is listed on the right. **e, f** Control HEK 293T cells (lane 1) or HEK 293T cells stably expressing alt-RPL36-FLAG-HA (lane 2) were transfected with TMEM24 truncation mutants, and IPs were performed with anti-FLAG antibody followed by IB with anti-myc. **g** Control HEK 293T cells (lane 1), HEK 293T cells stably expressing wild-type alt-RPL36-FLAG-HA (lane 2), and HEK 293T cells stably expressing nonphosphorylatable 4S-A mutant alt-RPL36-FLAG-HA (lane 3) were transfected with the TMEM24 SMP + C2 domain construct, followed by IP with anti-FLAG antibody and immunoblotting with antibodies indicated on the right. Cell lysates (1%) before IP (input) were used as the loading controls. All western blots are representative of three biological replicates. **h** alt-RPL36-GFP11-FLAG KI cells were transfected with TMEM24-GFP, followed by immunostaining with anti-GFP (red), anti-FLAG (green) and DAPI (cyan). Scale bar, 10  $\mu\text{m}$ . Data are representative of three biological replicates. **i** Confocal imaging of alt-RPL36-GFP11-FLAG KI cells stably expressing control shRNA (sh-Ctrl, top panel) or TMEM24 shRNA (sh-TMEM24, bottom panel) after immunostaining with anti-Grp94 (red), anti-FLAG (green), and DAPI (cyan). Scale bar, 10  $\mu\text{m}$ . The arrow indicates the plane used for line profile generation. Right: line profiles of fluorescence intensities including Pearson correlation coefficients ( $r$ ). Data are representative of three biological replicates. **j** Pearson correlation coefficients of line profiles of Grp94 and alt-RPL36,  $N = 40$ . Significance was evaluated with two-tailed  $t$ -test. Source data are provided as a Source data file.

Third, we applied mRNA-seq to quantify the transcriptional state of wild-type vs. alt-RPL36 KO HEK 293T cells. We identified 329 genes significantly upregulated and 70 genes downregulated in the KO relative to wild-type ( $p < 0.05$ ,  $N = 2$ , Fig. 5e). KEGG analysis of genes upregulated in the KO revealed that GO term “PI3K-AKT signaling pathway” is enriched (Fig. 5f). To validate the mRNA-seq data, we performed qRT-PCR targeting three upregulated genes in the PI3K-AKT signaling pathway. As shown in Fig. 5g, all three genes are upregulated upon alt-RPL36 knockout, compared with wild-type HEK 293T cells, consistent with the mRNA-seq results. The upregulation can be partially rescued by complementary expression of wild-type, but not phosphorylation-incompetent, alt-RPL36 (Fig. 5g). Taken together, these results suggest that phosphorylated alt-RPL36 downregulates the PI3K-AKT-mTOR signaling pathway.

Our results demonstrate that alt-RPL36 KO cells have an increased pool of PM PI(4,5)P<sub>2</sub>, which leads to a small increase in PI3K pathway signaling under basal conditions. This further suggests that cells should exhibit increased activation of PI3K signaling downstream of receptor tyrosine kinase signaling, including EGFR, which is a physiological activator of the PI3K signaling pathway<sup>20</sup>. Consistent with this notion, alt-RPL36 KO HEK 293T cells are more sensitive to EGF stimulation, indicated by increased phosphorylation of AKT and its substrate, TSC2, after EGF treatment, compared with control cells (Supplementary Fig. 9).

Inhibition of mTOR has been reported to reduce cell size<sup>35,36</sup>. Because alt-RPL36 activates the mTOR pathway, we asked whether loss of alt-RPL36 could increase cell size. To this end, we measured the cellular volume of four cell lines (WT, KO, Rescue, and 4S-A rescue). As shown in Fig. 6a, b, knockout of alt-RPL36 indeed increased cell size, indicated by a larger cell volume, compared with wild-type HEK 293T cells. The increased cell size can be rescued by wild-type, but not phosphorylation-incompetent, alt-RPL36. These results indicate that alt-RPL36 downregulates cell size, consistent with inhibition of TMEM24 and the PI3K-AKT-mTOR pathway.

We noticed that the KO and 4S-A rescue HEK 293T cells showed a round morphology (Fig. 5a, rows 2 and 4), though this effect is only partially rescued by reintroduction of alt-RPL36 (Fig. 5a, row 3). We hypothesized that this could be caused by PI3K-dependent activation of the ROCK1 signaling pathway<sup>38–40</sup>, which induces cytoskeletal reorganization to promote cell motility. To confirm this hypothesis, we measured the

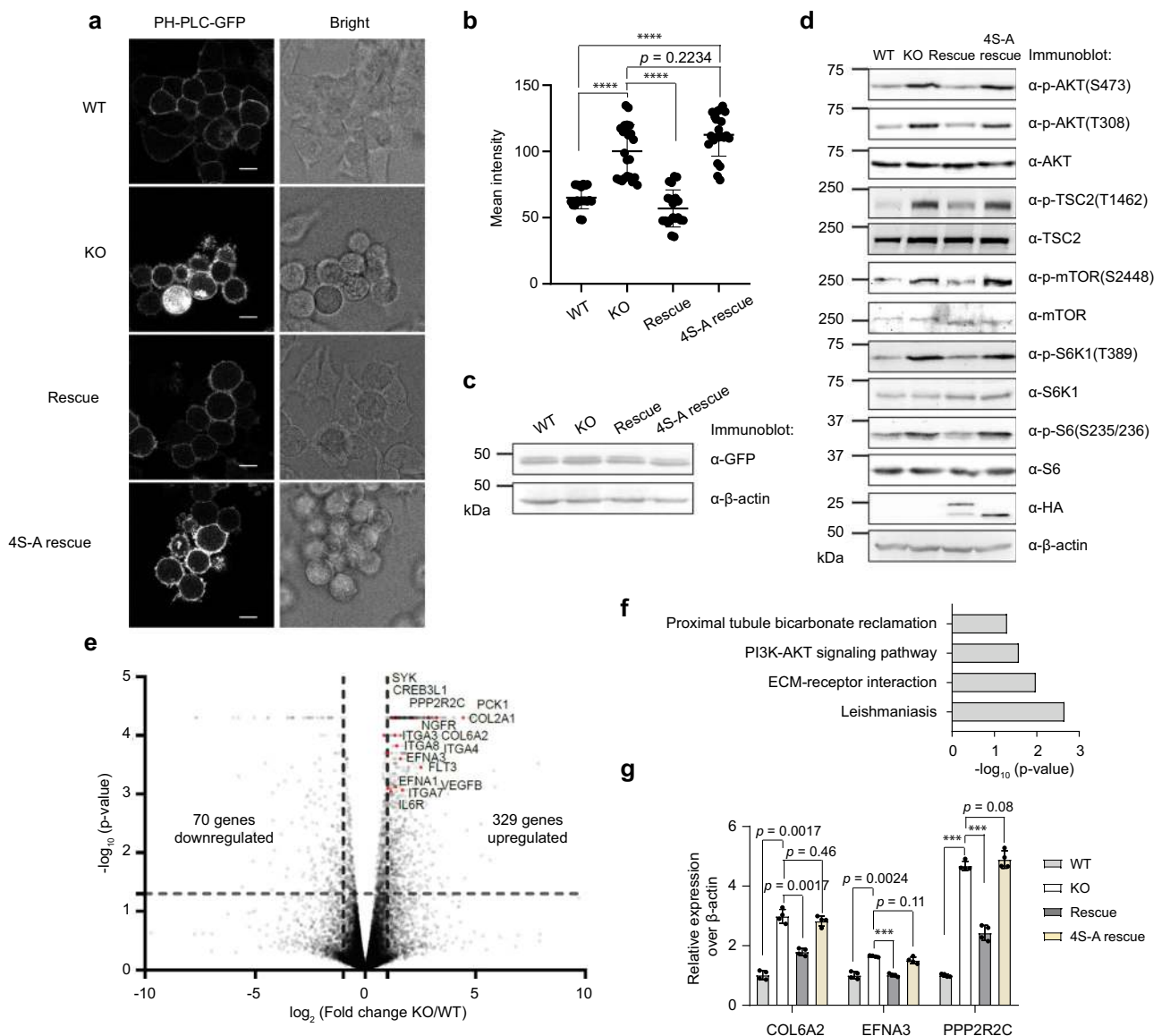
phosphorylation levels of two ROCK1 substrates, MLC2 and LIMK2. As shown in Fig. 6c, the phosphorylation of MLC2 and LIMK2 are upregulated upon alt-RPL36 knockout, and the upregulation can be partially rescued by wild-type, but not phosphorylation-incompetent, alt-RPL36. The observed rounding of the rescue cells may be due to incomplete rescue by alt-RPL36 reintroduction. Taken together, these results indicate that alt-RPL36 likely regulates cell morphology via the ROCK1 pathway.

**Regulation of PI3K-AKT-mTOR pathway by alt-RPL36 requires its interaction with TMEM24.** To determine whether regulation of PI3K-AKT-mTOR pathway by alt-RPL36 requires TMEM24, we knocked down TMEM24 with shRNA on the background of alt-RPL36 knockout (Fig. 7c, d), then measured PM PI(4,5)P<sub>2</sub> levels and PI3K-AKT-mTOR pathway phosphorylation. As shown in Fig. 7a, b, knockout of alt-RPL36 increased PI(4,5)P<sub>2</sub> levels compared to wild-type HEK 293T when transfected with a control shRNA (sh-Ctrl), as expected. Knockdown of TMEM24 on the alt-RPL36 KO background partially rescued the increase of PI(4,5)P<sub>2</sub> compared to transfection of alt-RPL36 KO cells with sh-Ctrl. These results indicate that alt-RPL36-dependent regulation of PI(4,5)P<sub>2</sub> levels require TMEM24. Similarly, as shown in Fig. 7d, while knockout of alt-RPL36 increased phosphorylation levels of PI3K-AKT-mTOR pathway kinases and substrates compared to wild-type (compare lane 2 with lane 1), knockdown of TMEM24 in alt-RPL36 KO partially rescued the increases (compare lane 4 with lane 2), again indicating that alt-RPL36-dependent regulation of PI3K-AKT-mTOR pathway requires TMEM24.

To further confirm these results, we knocked out TMEM24 in alt-RPL36 KO cells by transfecting them with Cas9 lentivirus and a guide RNA targeting TMEM24. We then measured PM PI(4,5)P<sub>2</sub> levels and the phosphorylation levels of the kinases and substrates of the PI3K-AKT-mTOR pathway, and observed similar results (Supplementary Fig. 10). Taken together, these results confirm that the regulation of PI3K-AKT-mTOR pathway by alt-RPL36 requires its interaction with TMEM24.

It is important to note that knockdown of TMEM24 alone in wild-type HEK 293T cells did not significantly change PM PI(4,5)P<sub>2</sub> levels (Fig. 7a and Supplementary Fig. 9a, compare row 3 with row 1) or activation of the PI3K-AKT-mTOR pathway (Fig. 7d and Supplementary Fig. 9d, compare lane 3 with lane 1). We hypothesize that this could be because TMEM24 is nearly completely inhibited by alt-RPL36 under basal conditions in cultured HEK 293T cells.





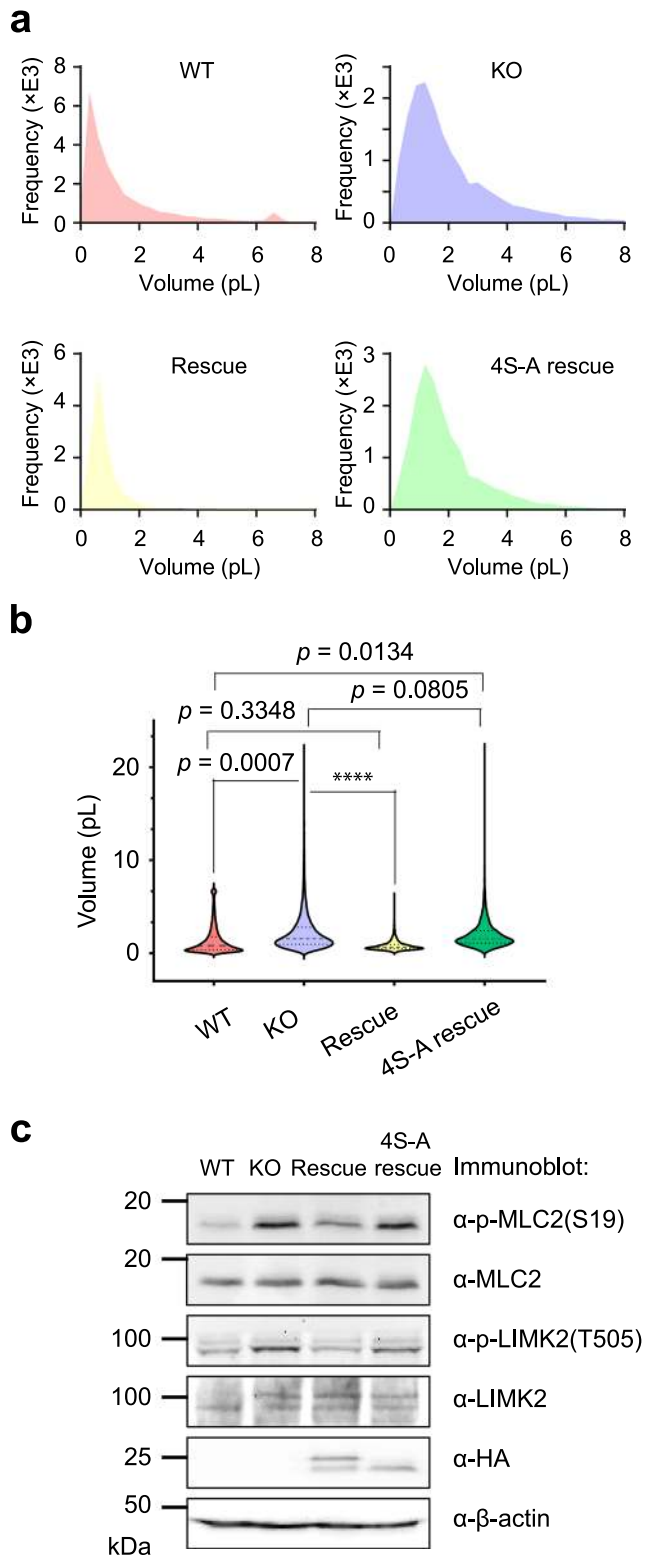
**Fig. 5** Phosphorylated alt-RPL36 regulates the PI3K-AKT-mTOR signaling pathway. **a** Confocal live-cell imaging of wild-type (WT), alt-RPL36 knockout (KO), rescue with wild-type alt-RPL36 (Rescue) or rescue with nonphosphorylatable 4S-A mutant alt-RPL36 (4S-A rescue) HEK 293T cells stably expressing PH-PLC-GFP. Scale bar, 10  $\mu$ m. Data are representative of three biological replicates. **b** Quantitation of the PH-PLC-GFP signals in the four cell lines described above. At least 20 fields of view were analyzed, totaling >400 cells for each measurement. Data represent mean values  $\pm$  s.e.m., and significance was evaluated with two-tailed *t*-test. \*\*\*\**p* < 0.0001. Source data are provided as a Source data file. **c** Western blot of the four cell lines with antibodies indicated on the right for comparison of PH-PLC-GFP expression. Data are representative of three biological replicates. **d** Western blot analysis of the wild-type (WT), alt-RPL36 knockout (KO), rescue with wild-type alt-RPL36-FLAG-HA (Rescue) or rescue with 4S-A mutated alt-RPL36-FLAG-HA (4S-A rescue) HEK 293T cells with antibodies indicated on the right. Data are representative of three biological replicates. **e** Volcano plot of mRNA-seq from wild-type (WT) and alt-RPL36 knockout (KO) HEK 293T cells. Upregulated transcriptional targets of the PI3K-AKT-mTOR signaling pathway identified via KEGG analysis are indicated in red and gene names are labeled. Significance was evaluated with Cuffdiff (two-tailed *t*-test). Source data are provided as a Source data file. **f** KEGG analysis of genes upregulated upon alt-RPL36 knockout; enriched biological pathways are plotted by significance (Fisher’s one-tailed test). **g** Quantitative RT-PCR results of PI3K-Akt pathway target transcripts in wild-type (WT), alt-RPL36 knockout (KO), rescue with wild-type alt-RPL36-FLAG-HA (Rescue) or rescue with 4S-A mutated alt-RPL36-FLAG-HA (4S-A rescue) HEK 293T cells. Data represent mean values  $\pm$  standard error of the mean (s.e.m.) of four biological replicates. Significance was evaluated with two-tailed *t*-test. \*\*\**p* < 0.001. Source data are provided as a Source data file.

**Cancer-related mutations affect alt-RPL36 protein properties and interaction.**

A number of cancer-associated point mutations in the human *RPL36* gene have been previously reported, and we queried whether any of these mutations could alter the sequence of alt-RPL36 (Supplementary Fig. 11a). Of 10 cancer-specific point mutations in the (alt-)RPL36 coding region (CDS) in the COSMIC database (cancer.sanger.ac.uk)<sup>41</sup>, 2 alter the amino acid

sequence of RPL36 but are synonymous in the alt-RPL36 reading frame; 4 affect both the RPL36 and alt-RPL36 amino acid sequences; and, remarkably, 4 are synonymous with respect to RPL36 but create nonsynonymous mutations in the alt-RPL36 reading frame.

To determine whether any of these mutations affect the properties or function of alt-RPL36, we generated HEK 293T

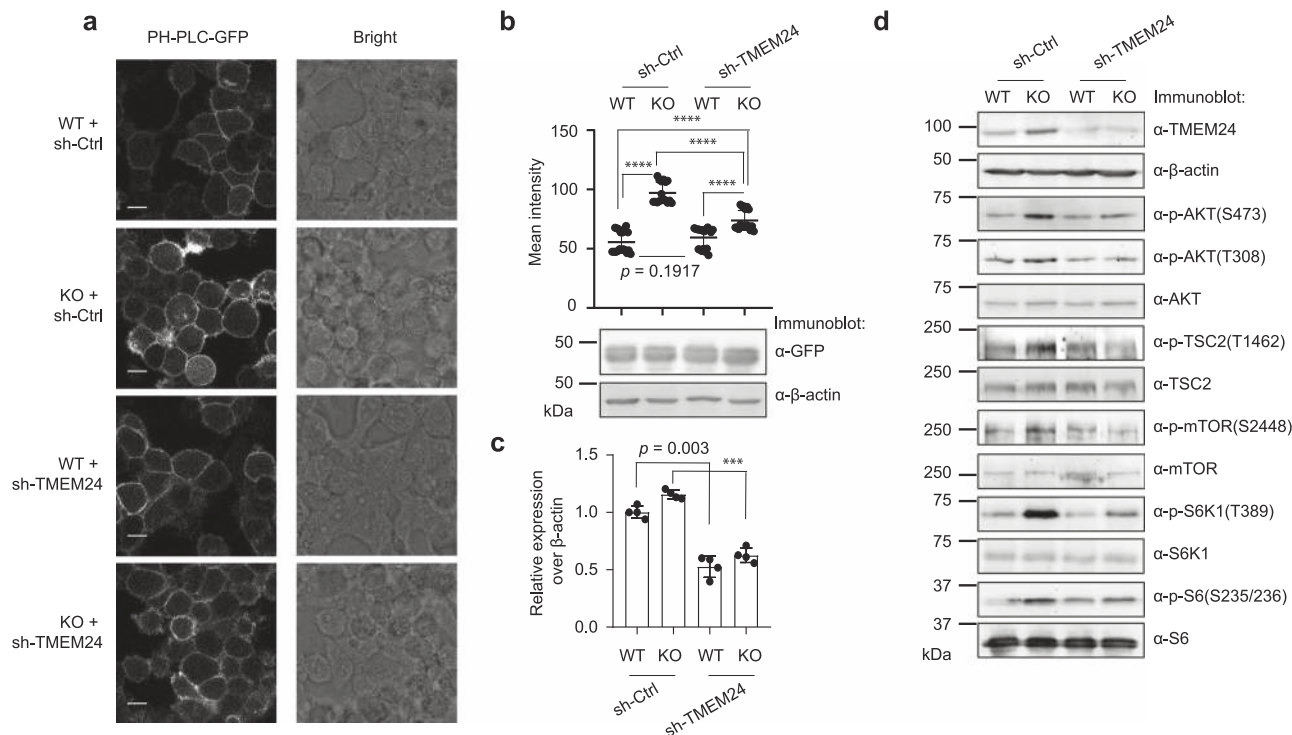


**Fig. 6 alt-RPL36 regulates cell size and morphology.** **a** Cell volume histogram for wild-type (WT), alt-RPL36 knockout (KO), rescue with wild-type alt-RPL36-FLAG-HA (Rescue), or rescue with nonphosphorylatable 4S-A mutant alt-RPL36-FLAG-HA (4S-A rescue) HEK 293T cells. **b** Violin plot of the cell volume of the four cell lines described above. Significance was evaluated with non-parametric Mann-Whitney two-tailed test. \*\*\*\* $p < 0.0001$ . Source data are provided as a Source data file. **c** Western blot of the four cell lines indicated at the top with the antibodies indicated to the right. Data are representative of three biological replicates.

stable cell lines expressing seven cancer-associated alt-RPL36 mutants. We first examined their effect on protein expression. As shown in Supplementary Fig. 11b, four-point mutations (V93A, S50N, Q98H, and P115A) exhibited reduced protein levels relative to the wild-type alt-RPL36 sequence. The mRNA profile of these mutants did not match the protein levels, suggesting that altered protein expression may be post-transcriptionally regulated (Supplementary Fig. 11c). Second, we examined the phosphorylation state of these mutants via Phos-tag western blotting. As shown in Supplementary Fig. 11d, 5 of the 7 mutants (V93A, S50N, Q98H, Q104H, and P115A) changed the phosphorylation pattern of alt-RPL36. The E118K mutation changed the mobility of all alt-RPL36 protein bands in the Phos-tag western blot, likely by changing the overall charge state of the protein. Finally, we tested the ability of each alt-RPL36 mutant to interact with TMEM24. As shown in Supplementary Fig. 11e, the S50N mutation essentially abolished the interaction, and other four mutations (R73C, Q98H, Q104H, and P115A) reduced the interaction. Taken together, these results suggest that several cancer-associated alt-RPL36 variants exhibit altered expression and phosphorylation, which may affect alt-RPL36 function. In the case of the melanoma-associated S50N variant, the observed loss-of-function with respect to TMEM24 interaction would be expected to derepress TMEM24.

## Discussion

In this work, we have identified a previously unannotated protein, alt-RPL36, that is co-encoded with human ribosomal protein L36 in the  $-1$  reading frame of *RPL36* transcript variant 2. Alt-RPL36 initiates at a non-AUG start codon upstream of the RPL36 initiation site and terminates downstream of the RPL36 stop codon, and both of these sequence-independent proteins are expressed from the same mRNA. Previous reports have demonstrated that upstream ORFs with non-AUG start codons tend to exhibit positively correlated expression with downstream coding sequences<sup>42</sup>, while upstream AUG start codons strongly inhibit translation of downstream cistrons<sup>43</sup>. Therefore, because alt-RPL36 initiates at a non-AUG start site, it does not efficiently repress translation of RPL36, allowing the two proteins to be translated from the same mRNA. Despite their co-expression, alt-RPL36 is likely present in cells at a significantly lower concentration than RPL36, though we have not yet directly quantified its cellular copy number. The *RPL36* transcript variant 2-specific exon is  $\sim 10$ -fold less abundant than an exon specific to transcript variant 1, which only encodes RPL36, according to quantitative RNA-seq (Supplementary Fig. 7a). Further taking into account  $\sim 10$ -fold less efficient translation initiation at GUG start codons relative to AUG<sup>44</sup>, there is likely to be at least 100-fold less alt-RPL36 in the cell than RPL36. Notwithstanding their differing cellular abundances, RPL36—a ribosomal protein—and alt-RPL36—a negative regulator of the PI3K–AKT–mTOR signaling pathway—regulate the same process (protein translation) via different mechanisms, and in different directions. While many human smORFs are now hypothesized to exist in bicistronic transcripts that function as operons<sup>12,14</sup>, few examples of co-encoded human proteins have been characterized in molecular detail. This includes bicistronically-encoded fatty acid synthesis and RNA processing proteins HsHTD2 and RPP14, and overlapping open reading frames encoding RNA-binding proteins and interactors ATXN1/Alt-ATXN1<sup>45,46</sup>. This work, combined with previous literature, expands the recent finding that dense co-encoding of functionally related proteins within the same transcript—and even within overlapping nucleotide sequences—can occur in the human genome<sup>45–48</sup>.



**Fig. 7 Regulation of PI3K-AKT-mTOR pathway by alt-RPL36 requires its interaction with TMEM24.** **a** PH-PLC-GFP reporter was stably introduced into the following cell lines: HEK 293T cells stably expressing control shRNA (WT + sh-Ctrl), alt-RPL36 KO cells stably expressing control shRNA (KO + sh-Ctrl), HEK 293T stably expressing TMEM24 shRNA (WT + sh-TMEM24), alt-RPL36 KO stably expressing TMEM24 shRNA (KO + sh-TMEM24). Confocal imaging was performed with live cells. Scale bar, 10  $\mu$ m. Data are representative of three biological replicates. **b** Top: quantitation of the PH-PLC-GFP signals in the four cell lines described above. At least 16 fields of view were analyzed, totaling >300 cells for each measurement. Data represent mean values  $\pm$  s.e.m., and significance was evaluated with two-tailed *t*-test. \*\*\*\* $p < 0.0001$ . Source data are provided as a Source data file. Bottom: western blot of the four cell lines with antibodies indicated on the right for comparison of PH-PLC-GFP expression. Data are representative of three biological replicates. **c** Quantitative RT-PCR with primers specific to TMEM24 to assess efficiency of silencing by sh-TMEM24 (error bars, standard error of the mean (s.e.m.),  $N = 4$  biologically independent samples, \*\*\* $p < 0.001$  (two-tailed *t*-test)). Source data are provided as a Source data file. **d** Western blot analysis of the four cell lines described above with antibodies indicated on the right. Data are representative of three biological replicates.

Because the alt-RPL36 and RPL36 coding sequences overlap, conservation of alt-RPL36 may be challenging to detect. Furthermore, it is not yet clear whether alternative splice variants of *RPL36* exist, or are annotated, in different species. Expression of putative homologs in other mammalian species must be experimentally tested. It is also possible that alt-RPL36 represents an example of a *de novo* evolved gene<sup>49,50</sup>. Functional *de novo* evolved genes have been previously detected in plants and animals, wherein they function in reproduction and development and are differentially expressed in response to stress<sup>51,52</sup>.

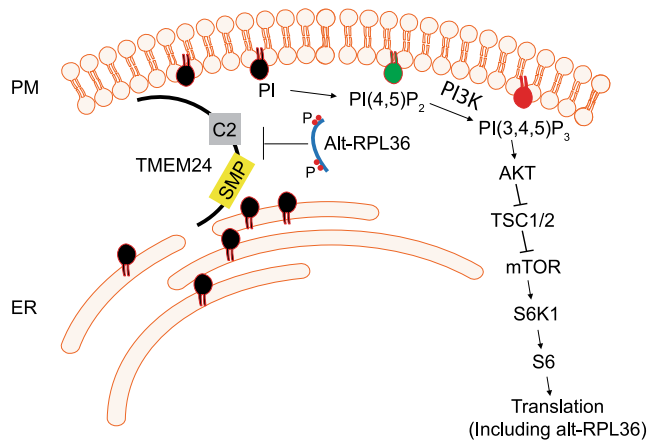
Previous proteomic studies have detected phosphorylated peptides mapping to alt-proteins in cells undergoing mitosis and stimulation by EGF<sup>13,53</sup>. This data strongly suggests that alt-ORFs may be functional and regulated by post-translational modifications. The discovery that alt-RPL36 is highly phosphorylated, and that its association with its target protein requires these phosphoserine residues, further supports the notion that additional sm/alt-ORF-encoded proteins bear functional modifications. Similar to TMEM24<sup>18,22</sup>, phosphorylation of alt-RPL36 is also dynamically regulated by the cytosolic calcium level. While we have not yet explored the functional consequence of this regulation, considered together with the observation that alt-RPL36 phosphorylation is required for TMEM24 association, these results suggest that repression of TMEM24 by phosphorylated alt-RPL36 could potentially be reversible under some physiological conditions.

The discovery of alt-RPL36 provides opportunities for investigating dynamic upstream regulation of the PI3K-AKT-mTOR

pathway, an overall model of which is provided in Fig. 8. Phosphorylated (P) alt-RPL36 interacts with and negatively regulates TMEM24-dependent phosphatidylinositol (PI) transport. In cells lacking alt-RPL36, or, hypothetically, cells in which alt-RPL36 phosphorylation is reduced, TMEM24 is released from inhibition by alt-RPL36, increasing PI transport to the plasma membrane and subsequent conversion to PI(4,5)P<sub>2</sub> and PI(3,4,5)P<sub>3</sub>—the latter via the activity of PI3K. PI(3,4,5)P<sub>3</sub> activates AKT, leading to activation of downstream mTOR signaling, and upregulates protein translation—likely including translation of alt-RPL36. The resulting increase in alt-RPL36 then inhibits TMEM24, restoring homeostasis. We note that additional biological assays will be required to establish whether alt-RPL36 is a physiologically relevant regulator of mTOR signaling.

The subcellular localization of alt-RPL36 may be relevant to its function, but several questions remain to be answered. TMEM24 has been reported to localize to ER-PM contact sites, and to relocalize throughout the ER when its C-terminal domain is phosphorylated<sup>22</sup>. The observation that endogenously expressed alt-RPL36 localizes to the pan-ER, but is enriched at PM contact sites when over-expressing TMEM24, is consistent with TMEM24 binding. However, further work is needed to determine whether, like TMEM24, alt-RPL36 relocalizes under physiological conditions, and whether its subcellular localization is regulated by its phosphorylation state under physiological conditions.

Finally, our functional data demonstrate that the cellular phenotypes associated with alt-RPL36 ablation require TMEM24, conclusively establishing TMEM24 as the direct functional target



**Fig. 8 Model of alt-RPL36 regulatory pathway.** Phosphorylated (P) alt-RPL36 interacts with TMEM24 via the SMP and C2 domains to negatively regulate TMEM24-dependent phosphatidylinositol 4,5-bisphosphate [PI(4,5)P<sub>2</sub>] precursor phosphatidylinositol (PI) transport. In cells lacking alt-RPL36, TMEM24 is released from the inhibition by alt-RPL36, and more PI is transported to the plasma membrane (PM) from the endoplasmic reticulum (ER), where it is synthesized. At the PM, PI is converted to PI(4,5)P<sub>2</sub> then phosphorylated by PI3K to produce PI(3,4,5)P<sub>3</sub>. PI(3,4,5)P<sub>3</sub> then activates AKT, which phosphorylates and inhibits TSC1/2, then activates downstream mTOR signaling. mTOR phosphorylates S6K1, and activated S6K1 phosphorylates S6, finally upregulates protein translation, including alt-RPL36. Upregulated alt-RPL36 then inhibits TMEM24, restoring homeostasis.

of alt-RPL36. These data furthermore suggest that alt-RPL36 inhibits TMEM24. However, the functional assays employed in this study are indirect readouts of TMEM24 activity. Therefore, the mechanism by which phosphorylated alt-RPL36 inhibits TMEM24 remains to be established. It is possible that the alt-RPL36 interaction with the SMP and C2 domains of TMEM24 affects its lipid transport activity, either by competitive binding or conformational change. It is alternatively possible that phosphorylated alt-RPL36 contributes to electrostatic inhibition of the TMEM24-PM interaction, thereby interfering with phospholipid transport between these membranes by altering TMEM24 localization. A similar electrostatic inhibitory effect leading to PM dissociation has been shown to occur upon phosphorylation of the TMEM24 C-terminus<sup>18,22</sup>. Simpler mechanisms, such as alteration of the stability or folding of TMEM24 by alt-RPL36, are also possible. Further cell-based, biochemical and structural studies will be required to differentiate these possible mechanisms of action.

## Methods

**Data analysis.** Statistics, two-tailed *t*-test was performed using Excel or Prism, and equal variance between samples being compared was established using an *F*-test.

**Antibodies and reagents.** Primary antibodies for western blotting include the following: anti-FLAG (1:500, Sigma, F3165); anti-myc (1:1000, Rockland, 600-401-381, 1:1000, Cell Signaling, 2276 (mouse), or 1:1000, Cell Signaling, 2278 (rabbit)); anti-HA (1:3000, Invitrogen, 71-5500); anti-His (1:1000, Thermo Fisher, MA1-21315); anti-V5 (1:1000, Cell Signaling, 13202); anti-β-actin (1:2000, Invitrogen, BA3R); anti-p-mTOR(S2448) (1:500, Cell Signaling Technology, 2971); anti-mTOR (1:500, Cell Signaling Technology, 2972); anti-p-AKT(S473) (1:1000, Cell Signaling Technology, 9271); anti-p-AKT(T308) (1:1000, Cell Signaling Technology, 4056); anti-AKT (1:1000, Cell Signaling Technology, 9272); anti-p-TSC2 (T1462) (1:500, Cell Signaling Technology, 3617); anti-TSC2 (1:500, Cell Signaling Technology, 4308); anti-p-S6K1(T389) (1:2000, Cell Signaling Technology, 9234); anti-S6K1 (1:2000, Cell Signaling Technology, 9202); anti-p-S6(S235/236) (1:3000, Cell Signaling Technology, 2211); anti-S6 (1:3000, Cell Signaling Technology, 2217); anti-p-MLC2(S19) (1:1000, Cell Signaling Technology, 3671); anti-MLC2 (1:1000, Cell Signaling Technology, 3672); anti-p-LIMK2(T505) (1:500, Cell

Signaling Technology, 3841); anti-LIMK2 (1:500, Cell Signaling Technology, 3845); anti-p-EGFR(Y1068) (1:1000, Abcam, ab40815); anti-EGFR (1:1000, Abcam, ab52894); anti-RPL36 (1:1000, Bethyl Laboratories, A305065A-M); anti-TMEM24 (1:500, a gift from Pietro De Camilli, Yale). Immunoprecipitation was performed with the following antibody beads: anti-FLAG M2 affinity gel (Sigma, A2220); anti-myc tag agarose beads (Sigma, A7470); anti-HA tag magnetic beads (Thermo Fisher, 88836). mTOR inhibitor Torin1 (Tocris, 4247), PKC inhibitor Bisindolylmaleimide II (Cayman, 11020), Thapsigargin (Sigma, T9033), L-Azidohomoalanine (Click Chemistry tools, 1066-1000), Biotin-alkyne (Click Chemistry tools, 1266-5). Human EGF protein (Abcam, ab9697).

**Cloning and genetic constructs.** A construct comprising the full 5'UTR of human RPL36 transcript variant 2 through the stop codon of alt-RPL36 was synthesized by Genscript with a myc epitope tag appended to the 3' end of the alt-RPL36 coding sequence, then subcloned into pcDNA3. For generation of HEK 293T cells stably expressing alt-RPL36, a dual FLAG and HA tag was appended to the 3' end of alt-RPL36 by PCR, and the GTG start codon was mutated to ATG. The dually tagged coding sequence was amplified by PCR, then cloned into pLJM1. The serine point mutations with a dual FLAG and HA tag were generated by ligating the PCR products into AgeI and EcoRI cloning sites in the pLJM1 vector. The full-length TMEM24 clone with a C-terminal FLAG epitope tag in pcDNA3 was purchased from Genscript. The truncations of TMEM24 were generated by PCR with a C-terminal myc epitope tag, then subcloned into pcDNA3. The TMEM24-GFP plasmid is a gift from Dr. Pietro De Camilli at Yale. The TMEM24-GFP plasmid was purchased from Addgene (a gift from Tobias Meyer, Stanford), then cloned into pLJM1 by PCR. pPB-MmPylRS-AF-4xPylT<sub>CUA</sub>, which expresses *M. maezi* pyrrolysyl-tRNA synthetase<sup>Y306A/Y384F</sup> (PylRS-AF) and 4 copies of pyl tRNA<sub>CUA</sub>, was a gift from Jason Chin (MRC Laboratory of Molecular Biology, UK). pPB-alt-RPL36-4xPylT<sub>CUA</sub> was cloned via subcloning alt-RPL36 gene to replace MmPylRS-AF via restriction cloning. Site-directed mutagenesis to introduce L18TAG, A30TAG, and V31TAG mutations to alt-RPL36 were performed on pPB-alt-RPL36-4xPylT with standard protocols.

**Cell culture and transfection.** HEK 293T cells were purchased from ATCC and early-passage stocks were established in order to ensure cell line identity; cells were maintained up to only 10 passages. HEK 293T cells were cultured in DMEM (Corning, 10-013-CV) with 10% FBS (Sigma, F0392) and 1% penicillin-streptomycin (VWR, 97063-708) in a 5% CO<sub>2</sub> atmosphere at 37 °C. Plasmid transfection was performed with Lipofectamine 2000 or Lipofectamine 3000 and Opti-MEM (GIBCO, 31985-070) according to the manufacturer's instructions, or polyethyleneimine (PEI, Polysciences, 23966-1) according to established protocols<sup>54</sup>, and growth media were replaced after 3–5 h (Lipofectamine 2000 or 3000 transfection) or 7–8 h (polyethyleneimine transfection).

**Lentivirus production and stable cell line generation.** Lentivirus was produced as previously described<sup>55</sup>. Briefly, HEK 293T cells were co-transfected using Lipofectamine 2000 or polyethyleneimine with expression construct in pLJM1, along with pMD2.G and psPAX2, and growth media were replaced after 3–5 h (Lipofectamine 2000 transfection) or 7–8 h (polyethyleneimine transfection). 48 h post transfection, media containing viruses was harvested, filtered through a 0.45-μm filter, and infection was performed by mixing with two volumes of fresh media containing suspended HEK 293T cells. Twenty-four hours post-infection, the growth media was replaced. Forty-eight hours post-infection, stably expressing cells were selected with 6 μg/mL puromycin for 2 days. Early stocks of stable cell lines were established after selection. Stable cell lines were released from puromycin for 2 days prior to use in experiments.

**Alt-RPL36 labeling and imaging.** HEK 293T cells were seeded onto 6-well plates for western blot analysis or on glass coverslips placed in 24-well plates for imaging studies. The coverslips were incubated for 1 h with 0.1 mg/mL poly-D-lysine. Upon reaching ~80% confluency, the media was exchanged for Opti-MEM containing transfection mixture of DNA (plasmid ratio of pPB-alt-RPL36-4xPylT<sub>CUA</sub>:pPB-mPylRS-AF-4xPylT<sub>CUA</sub> = 9:1), Lipofectamine 3000, and its accessory reagent (Thermo Fisher). After incubation for 6 h at 37 °C, the media was exchanged for DMEM supplemented with 10% FBS, 1% Pen-strep, and 60 μM BCNK (Sichem). Subsequently, cells were grown in presence of BCNK for 45 h. To analyze BCNK-bearing alt-RPL36 expression, cells were lysed with RIPA buffer, and lysates resolved on polyacrylamide gels. Proteins were transferred onto nitrocellulose membranes, and western blotting with anti-myc antibody was performed using standard protocols and imaged with ImageQuant LAS500 (GE Healthcare).

To fluorescently label alt-RPL36 via inverse-electron-demand Diels-Alder cycloaddition, cells were grown in BCNK-free media for another 3–6 h to remove excess BCNK. Thereafter, 800 nM tetrazine-SiR (Spirochrome) was incubated with the cells in regular growth media at 37 °C for 30 min. To stain the ER, 0.5 μM of ER tracker Blue-White DPX dye (Thermo Fisher) was added simultaneously with tetrazine-SiR. Cells were washed extensively with PBS prior to live-cell imaging on an Olympus Fluoview FV3000 confocal microscope with 63× oil immersion objective under atmosphere-controlled stage at 37 °C and appropriate laser and filter settings, and analyzed with cellSens Software.

To determine whether alt-RPL36 is co-localized with ER marker Grp94, line profile analysis was performed. Line profiles were generated with FIJI (ImageJ). For each cell, two straight lines were drawn to cross the ER in different directions, indicated by the arrows shown in the figures. Fluorescence signals along the straight line of ER and examined proteins were calculated with the plot profile tool in FIJI. The Pearson's correlation coefficient  $r$  values of two fluorescence signals were calculated with Excel. Perfect co-localization is indicated by  $r = 1$ , perfect exclusion is indicated by  $r = -1$ , and 0 means random distribution.

**PH-PLC-GFP imaging.** HEK 293T cells stably expressing PH-PLC-GFP were grown to 80% confluency on coverslips in 12-well plates. Coverslips were inverted and imaged in pre-warmed DMEM with 10% FBS, 1% penicillin-streptomycin in MatTek imaging dishes. Confocal imaging was performed on a Leica SP8 LS confocal microscope with 63× oil immersion objective under atmosphere-controlled stage at 37 °C. Quantification was performed with Image J using standard parameters.

**Co-immunoprecipitation.** HEK 293T cells were grown to 50% confluency in 15-cm dishes, then transiently transfected with the indicated plasmids. Forty-eight hours after transfection, cells were harvested and suspended in 1 mL lysis buffer (Tris-buffered saline (TBS) with 1% Triton X-100 and Roche Complete protease inhibitor cocktail tablets). Then cells were sonicated (50% intensity, 5 s pulse with 25 s rest, 5×, MICROSON XL 2000) on ice followed by centrifugation at 21,130 ×g, 4 °C, 10 min. One percent of lysate samples were saved for analysis of loading. A 25 μL aliquot of anti-FLAG agarose beads (clone M2, Sigma) was washed with 1 mL lysis buffer, collected by centrifugation for 2 min at 1000 ×g, then suspended in the cell lysate supernatant. Beads suspensions were rotated at 4 °C for 1 h, then washed three times with wash buffer (Tris-buffered saline (TBS) with 1% Triton X-100 and 350 mM NaCl), then 1 time with lysis buffer. Proteins were eluted by adding 40 μL SDS-PAGE loading buffer and boiling.

**Immunoprecipitation and proteomics.** Control HEK 293T cells or HEK 293T cells stably expressing alt-RPL36-FLAG-HA were grown to 80–90% confluency in 15-cm dishes. Cells were harvested and immunoprecipitation was performed as described above. After the final wash, elution was in 40 μL of 3× FLAG peptide (Sigma), at a final concentration of 100 μg/mL in lysis buffer at 4 °C for 1 h. Beads were removed by centrifugation and the entire supernatant were collected. A 50 μL aliquot of anti-HA magnetic beads (Cat.88836, Thermo Fisher) was washed with 1 mL lysis buffer, then suspended in the elution. Bead suspensions were rotated at 4 °C for 4 h, then washed three times with lysis buffer. Elution was in 40 μL of HA peptide (Covance), at a final concentration of 400 μg/mL in lysis buffer at 4 °C for 2 h. The eluted proteins were subjected to MS-MS analysis.

**Proteomics and database searches.** Protein-containing gel slices were digested with trypsin at 37 °C for 14–16 h. The resulting peptide mixtures were extracted from the gel, dried, followed with ethyl acetate extraction to remove residual detergent, then re-suspended in 15 μL of 3:8 70% formic acid:0.1% TFA. A 5 μL aliquot of each sample was injected onto a pre-packed column attached to a nanoAcquity UPLC (Waters) in-line with an LTQ Orbitrap Velos (Thermo Scientific) and a 90-min gradient was used to further separate the peptide mixtures as follows (solvent A: 0.1% formic acid; solvent B: acetonitrile with 0.1% formic acid): Single pump trapping was turned on for 6 min at a flow rate of 2.5 μL/min at 98% A. Isocratic flow was maintained at 0.3 μL/min at 2% B for 10 min, followed by linear gradients from 2% B to 10% B over 2 min, 10% B to 25% B over 58 min, 25% B to 40% B over 10 min, 40% B to 95% B over 2 min. Isocratic flow at 95% B was maintained for 5 min, followed by a gradient from 95% B to 2% B over 10 min. The column flow rate was 0.3 μL/min. The full MS was collected over the mass range of 298–1750  $m/z$  with a resolution of 30,000. MS/MS data were collected using a top 10 high-collisional energy dissociation method in data-dependent mode with a normalized collision energy of 33.0 eV and a 2.0  $m/z$  isolation window. The first mass was 100  $m/z$  in fixed mode. MS/MS resolution was 7500 and dynamic exclusion was 60 s.

For identification of alt- and microproteins, ProteoWizard MS Convert was used for peak picking and files were analyzed using Mascot Daemon (version 2.5.0.1). Oxidation of methionine and N-terminal acetylation were set as variable modifications, and a three-frame translation of mRNA-seq from HEK 293T cells was used as the database, as previously reported<sup>1</sup>. For co-IP proteomics searches and quantitative analysis, files were analyzed using MaxQuant (version 1.6.8.0), oxidation of methionine and N-terminal acetylation were set as variable modifications, and human UniProt (version 2019) plus alt-RPL36 was used as the database for searching. For phosphoproteomics searches, phosphorylation of Ser, Thr and Tyr, oxidation of methionine, and N-terminal acetylation were set as variable modifications. ProteoWizard MS Convert was used for peak picking and files were analyzed using Mascot Daemon (version 2.5.0.1), and human UniProt (version 2019) plus alt-RPL36 was used as the database. Two biological replicates were performed. For all analysis, a mass deviation of 20 p.p.m. was set for MS1 peaks, and 0.6 Da was set as the maximum allowed MS/MS peak with a maximum of two missed cleavages. Maximum false discovery rates (FDR) were set to 1% both

on peptide and protein levels. Minimum required peptide length was five amino acids. Protein quantitation was accomplished by calculating the LFQ intensity ratio of pulldown to negative control samples using MaxQuant (version 1.6.8.0) with standard parameters.

**Phos-tag SDS-PAGE and western blotting.** Phos-tag SDS-PAGE was performed with 10% polyacrylamide gels containing 50 μM Phos-tag acrylamide and 100 μM MnCl<sub>2</sub>. After electrophoresis, Phos-tag acrylamide gels were washed with transfer buffer containing 10 mM EDTA for 10 min with gentle shaking and then with transfer buffer without EDTA for 10 min according to the manufacturer's protocol. Proteins were transferred to nitrocellulose membranes followed by a standard western blotting protocol<sup>7</sup>. Briefly, Immunoblots were blocked with 3% BSA in TBS-T for 1 h at room temperature (RT), then probed with primary antibodies in the same buffer overnight at 4 °C. The membrane was washed three times with TBS-T, then probed with secondary antibodies in 3% BSA in TBS-T for 1 h at RT, then washed three times with TBS-T before development with Clarity ECL Western Blotting Substrate (Bio-Rad) and imaging. The uncropped blots are shown in Supplementary Figs. 14–20.

**Phosphatase treatment.** Alt-RPL36-FLAG-HA expressed and immunopurified from HEK 293T cells was incubated with 0.4 U/μL alkaline phosphatase, calf intestinal (CIP) (NEB, cat. M0290) at 37 °C for 1 h, or 8 U/μL lambda protein phosphatase (NEB, cat. P0753) at 30 °C for 0.5 h according to the manufacturer's instructions in a total reaction volume of 20 μL before western blotting.

**Recombinant expression and purification of human alt-RPL36.** His-MBP-tagged human alt-RPL36 in pET21a was transformed into an *E. coli* BL21 (DE3) strain. Overnight cultures were diluted 1:500 in Luria-Bertani (LB) media supplemented with 100 μg/mL of ampicillin and grown at 37 °C. Expression was induced by adding 0.5 mM of isopropyl β-d-1-thiogalactopyranoside (IPTG) when OD 600 reached 0.6, followed by shaking at 18 °C overnight. After cell harvest and resuspension in lysis buffer (50 mM Tris-HCl pH 7.5, 300 mM NaCl, 2 mM imidazole) with 1 mM β-mercaptoethanol and Roche Complete protease inhibitor cocktail tablets, cells were lysed by sonication (30% intensity, 10 s pulse with 50 s rest on ice, 20×). The solution was clarified by centrifugation at 34,520 ×g for 20 min at 4 °C and loaded onto a column containing 1 mL of Co<sup>2+</sup>-TALON resin (Takara, 635606) pre-equilibrated with lysis buffer. Following incubation for 1 h at 4 °C, the resin was washed with 10 mL of lysis buffer and 30 mL wash buffer (50 mM Tris-HCl pH 7.5, 300 mM NaCl, and 10 mM imidazole), and proteins were eluted with elution buffer (50 mM Tris-HCl pH 7.5, 300 mM NaCl and 250 mM imidazole). Eluted proteins mixed with 15% glycerol were snap-frozen and stored at –80 °C.

**In vitro phosphorylation.** In vitro alt-RPL36 phosphorylation by PKCα (Invitrogen, P2232) was performed by incubating various concentrations (0–0.3 μM) of PKCα with 2 μM purified His-MBP-alt-RPL36 in reaction buffer (20 mM HEPES-KOH pH 7.4, 16.7 mM CaCl<sub>2</sub>, 10 mM DTT, 100 mM NaCl, 100 μM ATP, and 0.6 mg/mL phosphatidylerine) at 30 °C for 0.5 h in a total reaction volume of 10 μL.

**Generation of alt-RPL36 knockout and knock-in cell lines.** Alt-RPL36 KO and 3xGFP11-FLAG KI HEK 293T cells were generated using CRISPR-Cas9. Guide RNAs (gRNAs) were designed with the guide design tool from the Zhang lab ([crispr.mit.edu](http://crispr.mit.edu)) to target the RPL36 genomic region (gRNA1: 5'-CCGGGA-TATCTACTCGGCTC-3'; gRNA2: 5'-GAGTACCGGCTCAGTCCCG-3') for KO, and gRNA 5'-CCCGATAGTCGCCGCTCCGG-3' for KI. Double-stranded DNA oligonucleotides corresponding to the gRNAs were inserted into pSpCas9 (BB)-2A-GFP vector (Addgene, as a gift from F. Zhang, MIT, Cambridge, MA).

For generation of KO cells, an equal mixture of the two gRNA plasmids were transfected into HEK 293T cells using Lipofectamine 2000 (Invitrogen) according to the manufacturer's instructions, and GFP-positive cells were sorted with flow cytometry. Loss of alt-RPL36 expression was confirmed by genomic DNA PCR and sequencing. In the alt-RPL36 KO cell line used in this study, the two alleles were disrupted by a 210-nt homozygous deletion, deleting the alt-RPL36 start codon, but not the RPL36 start codon. And no large deletion or insertion were observed in the 100 kb upstream and 100 kb downstream of the edited sites, indicated by Xdrop long-read DNA sequencing (Supplementary Fig. 12 and Supplementary Data 4). Eleven predicted off-target sites were confirmed to be unedited by genomic PCR and sequencing (Supplementary Fig. 13 and Supplementary Data 5).

For generation of KI cells, a donor plasmid containing 300 bp homology left-arm and 300 bp homology right-arm sequence around the stop codon of alt-RPL36, which are separated with 3xGFP11-FLAG tag and BamHI/NotI restriction sites were synthesized from GenScript, a DNA sequence containing pGK promoter and hygromycin resistant gene was subcloned into the donor plasmid with BamHI and NotI. An equal mixture of the gRNA and donor plasmids were transfected into HEK 293T cells using Lipofectamine 2000 (Invitrogen) according to the manufacturer's instructions, and hygromycin selection was performed 2-day post

transfection. Alt-RPL36-3xGFP11-FLAG KI cells were confirmed by genomic DNA PCR and sequencing.

And no large deletion or insertion were observed in the 100 kb upstream and 100 kb downstream of the edited sites, indicated by Xdrop long-read DNA sequencing (Supplementary Fig. 12 and Supplementary Data 4).

**KO and KI cell line validation through Xdrop long-read DNA sequencing.** High molecular weight (HMW) DNA was isolated from alt-RPL36 knockout (KO) or knock-in (KI) cell lines using the Blood & Cell Culture DNA Mini Kit (Qiagen). Xdrop sequencing was performed by Samplix (Denmark). Briefly, HMW DNA was evaluated by the TapeStation™ System (Agilent Technologies Inc.), using Genomic DNA ScreenTape according to the manufacturer's instructions. The HMW DNA samples were further purified using HighPrep™ PCR Clean-up Bead System according to the manufacturer's instructions (MAGBIO Genomics) with the following changes: Bead-to-sample ratios were 1:1 (v:v) and elution was performed by heating the sample in elution buffer for 3 min at 55 °C before separation on the magnet. The samples were eluted in 20 µl 10 mM Tris-HCl (pH 8). Purified DNA samples were quantified by Quantus (Promega Inc.) Fluorometer™, according to the manufacturer's instructions. DNA was partitioned in droplets by Xdrop™ and subjected to PCR using the enrichment PCR assays. The primers were designed ~45 kb both up- and downstream of RPL36 on chromosome 19 with the aim of enriching 100 kb of DNA in either direction. Primers were localized to genes CATSPERD and SAFB at positions chr19:5,720,156–5,778,734 and chr19:5,623,035–5,668,478, respectively.

The droplet productions were then sorted by fluorescence-activated cell sorting (FACS). The isolated droplets were broken, and DNA was again partitioned in droplets by Xdrop™ and amplified by droplet multiple displacement amplification (dMDA) reactions. After amplification DNA was isolated and quantified. Minion Oxford Nanopore Sequencing platform was used to generate long-read sequencing data from the dMDA samples as described by the manufacturer's instructions (Premium whole genome amplification protocol (SQK-LSK109) with the Native Barcoding Expansion 1-12 (EXP-NBD104)). Generated raw data (FAST5) was subjected to basecalling using Guppy v.3.4.5 with high accuracy and quality filtering to generate FASTQ sequencing data. A minimum of 1 gigabyte of sequencing data was obtained from each sample. Raw reads were corrected using the necat.pl script from the package NECAT (v 0.0.1). Corrected reads were further split at chimeric positions using the SACRA pipeline (<https://github.com/hattori-lab/SACRA>) according to standard parameters. Finally, non-chimeric reads were mapped to GRCh38 chromosome 19 with ngmlr 0.2.7 and variants were called using sniffles 1.0.12 using parameters specific to ONT sequencing data<sup>56</sup>.

**Alt-RPL36 conservation analysis.** For alt-RPL36 conservation analysis, RPL36 mRNAs from different mammalian species were obtained from the NCBI nucleotide database, then translated in the +1, +2, and +3 frames using ExPaSy translate tool. Cognate or near-cognate start codons with in-frame Kozak consensus motifs were identified in the 5'UTR of each transcript, and were considered as the first amino acid (methionine) of alt-RPL36. The hypothetical proteins thus derived were aligned with Clustal Omega and visualized using JalView software using standard parameters.

**Cell size measurements.** The Scepter handheld cell counter (Millipore) was used to perform cell diameter and volume measurements on cells grown to 80–90% confluency and re-suspended in PBS to a concentration of  $1-5 \times 10^5$  cells/mL. Measurements were taken using a 60 µm sensor. Data were exported and visualized using Scepter Software Pro 2.1. Cell size distributions were compared for statistical differences using the non-parametric Mann–Whitney test.

**mRNA-seq and data analysis.** Whole RNA was isolated from  $2.5 \times 10^6$  control or alt-RPL36 knockout ( $N = 2$ ) HEK 293T cells using Qiagen RNeasy Mini Kit spin columns, then treated in solution with DNase I prior to Qiagen column clean-up according to the manufacturer's protocol. Whole RNA was submitted to the Yale Center for Genomic Analysis for preparation according to the standard Illumina protocol for paired-end sequencing with enrichment of poly-A RNA. Samples were multiplexed and 75 bp fragments were sequenced on the HiSeq2500 sequencer. The reads were mapped to the human genome (hg19) using TopHat (v2.0.11). To identify the genes regulated by alt-RPL36, we counted the RNA reads in exons and calculated the reads per kilobase per million reads (RPKM) for each gene as a measure of expression using Cufflinks (v.2.2.1) with the Cuffdiff tool using default parameters. A  $\log_2$  (fold change) cutoff of 0.2 with  $p$  value  $\leq 0.05$  was used to identify the genes with downregulated or upregulated expression in the alt-RPL36 knockout cells, compared with that in the control cells. Gene ontology analysis was performed using g:Profiler with standard parameters<sup>57</sup>. For qRT-PCR, total RNA was isolated using Trizol (Invitrogen) according to the manufacturer's protocol. Reverse transcription was performed with iScript (Bio-Rad) and qPCR was performed with iTaq Universal SYBR Green Supermix (Bio-Rad), with quantitation by a relative Ct method. qPCR primer sequences are provided in Supplementary Table 1.

**Reporting summary.** Further information on research design is available in the Nature Research Reporting Summary linked to this article.

## Data availability

The mRNA-seq and Xdrop sequence data have been deposited in the NCBI Gene Expression Omnibus under accession GSE144979. Proteomics data were deposited under accession PXD018268 to the PRIDE repository. Proteomics data associated with Figs. 1, 3, and 4 are included as Supplementary Data 1, 3, and 4, respectively. Additional conservation data are available from the corresponding author on request. Source data are provided with this paper.

Received: 17 March 2020; Accepted: 21 December 2020;

Published online: 21 January 2021

## References

- Cao, X. et al. Comparative proteomic profiling of unannotated microproteins and alternative proteins in human cell lines. *J. Proteome Res.* **19**, 3418–3426 (2020).
- Slavoff, S. A. et al. Peptidomic discovery of short open reading frame-encoded peptides in human cells. *Nat. Chem. Biol.* **9**, 59–64 (2013).
- Lee, S. et al. Global mapping of translation initiation sites in mammalian cells at single-nucleotide resolution. *Proc. Natl Acad. Sci. USA* **109**, E2424–E2432 (2012).
- Ingolia, N. T., Lareau, L. F. & Weissman, J. S. Ribosome profiling of mouse embryonic stem cells reveals the complexity and dynamics of mammalian proteomes. *Cell* **147**, 789–802 (2011).
- Saghatelian, A. & Couso, J. P. Discovery and characterization of smORF-encoded bioactive polypeptides. *Nat. Chem. Biol.* **11**, 909–916 (2015).
- Couso, J. P. & Patraquim, P. Classification and function of small open reading frames. *Nat. Rev. Mol. Cell Biol.* **18**, 575–589 (2017).
- D'Lima, N. G. et al. A human microprotein that interacts with the mRNA decapping complex. *Nat. Chem. Biol.* **13**, 174–180 (2017).
- Chu, Q. et al. Regulation of the ER stress response by a mitochondrial microprotein. *Nat. Commun.* **10**, 4883 (2019).
- Rathore, A. et al. MIEF1 microprotein regulates mitochondrial translation. *Biochemistry* **57**, 5564–5575 (2018).
- Jackson, R. et al. The translation of non-canonical open reading frames controls mucosal immunity. *Nature* **564**, 434–438 (2018).
- Anderson, D. M. et al. A micropeptide encoded by a putative long noncoding RNA regulates muscle performance. *Cell* **160**, 595–606 (2015).
- Chen, J. et al. Pervasive functional translation of noncanonical human open reading frames. *Science* **367**, 1140–1146 (2020).
- Samandi, S. et al. Deep transcriptome annotation enables the discovery and functional characterization of cryptic small proteins. *Elife* **6**, e27860 (2017).
- Brunet, M. A., Levesque, S. A., Hunting, D. J., Cohen, A. A. & Roucou, X. Recognition of the polycistronic nature of human genes is critical to understanding the genotype-phenotype relationship. *Genome Res.* **28**, 609–624 (2018).
- Aspden, J. L. et al. Extensive translation of small Open Reading Frames revealed by Poly-Ribo-Seq. *Elife* **3**, e03528 (2014).
- Wool, I. G., Chan, Y. L. & Gluck, A. Structure and evolution of mammalian ribosomal proteins. *Biochem. Cell Biol.* **73**, 933–947 (1995).
- Zhu, Y. et al. Discovery of coding regions in the human genome by integrated proteogenomics analysis workflow. *Nat. Commun.* **9**, 903 (2018).
- Lees, J. A. et al. Lipid transport by TMEM24 at ER-plasma membrane contacts regulates pulsatile insulin secretion. *Science* **355**, eaah6171 (2017).
- Fruman, D. A. et al. The PI3K pathway in human disease. *Cell* **170**, 605–635 (2017).
- Manning, B. D. & Toker, A. AKT/PKB signaling: navigating the network. *Cell* **169**, 381–405 (2017).
- Saxton, R. A. & Sabatini, D. M. mTOR signaling in growth, metabolism, and disease. *Cell* **168**, 960–976 (2017).
- Sun, E. W. et al. Lipid transporter TMEM24/C2CD2L is a Ca(2+)-regulated component of ER-plasma membrane contacts in mammalian neurons. *Proc. Natl Acad. Sci. USA* **116**, 5775–5784 (2019).
- Pottekat, A. et al. Insulin biosynthetic interaction network component, TMEM24, facilitates insulin reserve pool release. *Cell Rep.* **4**, 921–930 (2013).
- Kearse, M. G. & Wilusz, J. E. Non-AUG translation: a new start for protein synthesis in eukaryotes. *Genes Dev.* **31**, 1717–1731 (2017).
- Peabody, D. S. Translation initiation at non-AUG triplets in mammalian cells. *J. Biol. Chem.* **264**, 5031–5035 (1989).
- Cao, X. & Slavoff, S. A. Non-AUG start codons: expanding and regulating the small and alternative ORFeome. *Exp. Cell Res.* **391**, 111973 (2020).
- Uttamapinant, C., Supphakaw, K., Jantarug, K., Slavoff, S. & Israsena, N. A genetic code expansion-derived molecular beacon for the detection of intracellular amyloid-beta peptide generation. *Angew. Chem. Int. Ed. Engl.* <https://doi.org/10.1002/anie.202010703> (2020).

28. Wegener, A. D. & Jones, L. R. Phosphorylation-induced mobility shift in phospholamban in sodium dodecyl sulfate-polyacrylamide gels. Evidence for a protein structure consisting of multiple identical phosphorylatable subunits. *J. Biol. Chem.* **259**, 1834–1841 (1984).
29. Orr, M. W., Mao, Y., Storz, G. & Qian, S. B. Alternative ORFs and small ORFs: shedding light on the dark proteome. *Nucleic Acids Res.* **48**, 1029–1042 (2019).
30. Mellacheruvu, D. et al. The CRAPome: a contaminant repository for affinity purification-mass spectrometry data. *Nat. Methods* **10**, 730–736 (2013).
31. Chu, Q. et al. Identification of microprotein-protein interactions via APEX tagging. *Biochemistry* **56**, 3299–3306 (2017).
32. Slavoff, S. A., Heo, J., Budnik, B. A., Hanakahi, L. A. & Saghatelian, A. A human short open reading frame (sORF)-encoded polypeptide that stimulates DNA end joining. *J. Biol. Chem.* **289**, 10950–10957 (2014).
33. Davis, P. D. et al. Inhibitors of protein kinase C. 1. 2,3-Bisarylmaleimides. *J. Med. Chem.* **35**, 177–184 (1992).
34. Hogan, P. G., Lewis, R. S. & Rao, A. Molecular basis of calcium signaling in lymphocytes: STIM and ORAI. *Annu. Rev. Immunol.* **28**, 491–533 (2010).
35. Fingar, D. C., Salama, S., Tsou, C., Harlow, E. & Blenis, J. Mammalian cell size is controlled by mTOR and its downstream targets S6K1 and 4EBP1/eIF4E. *Genes Dev.* **16**, 1472–1487 (2002).
36. Fumarola, C., La Monica, S., Alfieri, R. R., Borra, E. & Guidotti, G. G. Cell size reduction induced by inhibition of the mTOR/S6K-signaling pathway protects Jurkat cells from apoptosis. *Cell Death Differ.* **12**, 1344–1357 (2005).
37. Varnai, P. & Balla, T. Visualization of phosphoinositides that bind pleckstrin homology domains: calcium- and agonist-induced dynamic changes and relationship to myo-[3H]inositol-labeled phosphoinositide pools. *J. Cell Biol.* **143**, 501–510 (1998).
38. Lien, E. C., Dibble, C. C. & Tokar, A. PI3K signaling in cancer: beyond AKT. *Curr. Opin. Cell Biol.* **45**, 62–71 (2017).
39. Wang, W., Eddy, R. & Condeelis, J. The cofilin pathway in breast cancer invasion and metastasis. *Nat. Rev. Cancer* **7**, 429–440 (2007).
40. Sanz-Moreno, V. et al. Rac activation and inactivation control plasticity of tumor cell movement. *Cell* **135**, 510–523 (2008).
41. Tate, J. G. et al. COSMIC: the catalogue of somatic mutations in cancer. *Nucleic Acids Res.* **47**, D941–D947 (2019).
42. Brar, G. A. et al. High-resolution view of the yeast meiotic program revealed by ribosome profiling. *Science* **335**, 552–557 (2012).
43. Calvo, S. E., Pagliarini, D. J. & Mootha, V. K. Upstream open reading frames cause widespread reduction of protein expression and are polymorphic among humans. *Proc. Natl Acad. Sci. USA* **106**, 7507–7512 (2009).
44. Wei, J., Zhang, Y., Ivanov, I. P. & Sachs, M. S. The stringency of start codon selection in the filamentous fungus *Neurospora crassa*. *J. Biol. Chem.* **288**, 9549–9562 (2013).
45. Bergeron, D. et al. An out-of-frame overlapping reading frame in the ataxin-1 coding sequence encodes a novel ataxin-1 interacting protein. *J. Biol. Chem.* **288**, 21824–21835 (2013).
46. Autio, K. J. et al. An ancient genetic link between vertebrate mitochondrial fatty acid synthesis and RNA processing. *FASEB J.* **22**, 569–578 (2008).
47. Andreev, D. E. et al. Translation of 5' leaders is pervasive in genes resistant to eIF2 repression. *Elife* **4**, e03971 (2015).
48. Vanderperre, B. et al. An overlapping reading frame in the PRNP gene encodes a novel polypeptide distinct from the prion protein. *FASEB J.* **25**, 2373–2386 (2011).
49. Andersson, D. I., Jerlstrom-Hultqvist, J. & Nasvall, J. Evolution of new functions de novo and from preexisting genes. *Cold Spring Harb. Perspect. Biol.* **7**, a017996 (2015).
50. Schlotterer, C. Genes from scratch—the evolutionary fate of de novo genes. *Trends Genet.* **31**, 215–219 (2015).
51. Donoghue, M. T., Keshavaiah, C., Swamidatta, S. H. & Spillane, C. Evolutionary origins of Brassicaceae specific genes in *Arabidopsis thaliana*. *BMC Evol. Biol.* **11**, 47 (2011).
52. Levine, M. T., Jones, C. D., Kern, A. D., Lindfors, H. A. & Begun, D. J. Novel genes derived from noncoding DNA in *Drosophila melanogaster* are frequently X-linked and exhibit testis-biased expression. *Proc. Natl Acad. Sci. USA* **103**, 9935–9939 (2006).
53. Sharma, K. et al. Ultradeep human phosphoproteome reveals a distinct regulatory nature of Tyr and Ser/Thr-based signaling. *Cell Rep.* **8**, 1583–1594 (2014).
54. Longo, P. A., Kavran, J. M., Kim, M. S. & Leahy, D. J. Transient mammalian cell transfection with polyethylenimine (PEI). *Methods Enzymol.* **529**, 227–240 (2013).
55. Tiscornia, G., Singer, O. & Verma, I. M. Production and purification of lentiviral vectors. *Nat. Protoc.* **1**, 241–245 (2006).
56. Sedlazeck, F. J. et al. Accurate detection of complex structural variations using single-molecule sequencing. *Nat. Methods* **15**, 461–468 (2018).
57. Raudvere, U. et al. g:Profiler: a web server for functional enrichment analysis and conversions of gene lists (2019 update). *Nucleic Acids Res.* **47**, W191–W198 (2019).

## Acknowledgements

We thank Benjamin Turk, Pietro de Camilli, and the members of the Slavoff lab for helpful discussions. This work was supported by an American Cancer Society Institutional Research Grant Individual Award for New Investigators (IRG-58-012-57), the Searle Scholars Program, an Odyssey Award from the Richard and Susan Smith Family Foundation, and Yale University West Campus start-up funds (to S.A.S.). X.C. was supported in part by a Rudolph J. Anderson postdoctoral fellowship from Yale University. A.K. was in part supported by an NIH Predoctoral Training Grant (5T32GM06754 3-12). T.P., K.S., and C.U. were supported by student and research assistant funds from VISTEC (to T.P. and K.S., respectively), a start-up grant from VISTEC (to C.U.), Thailand Research Fund (MRG6280177, to C.U.), and Seed Awards in Science from Wellcome Trust (to C.U.).

## Author contributions

X.C., A.K., Y.L., and E.O. designed and performed experiments and analyzed data. Z.N. designed and constructed CRISPR/Cas9 knockout cells. T.P. and K.S. performed unnatural amino acid labeling and live-cell imaging. C.U. designed experiments and analyzed data. S.A.S. conceived the project, designed experiments, and analyzed data. X.C., C.U., and S.A.S. wrote the manuscript, and all authors edited and approved the final version of the manuscript.

## Competing interests

The authors declare no competing interests.

## Additional information

**Supplementary information** is available for this paper at <https://doi.org/10.1038/s41467-020-20841-6>.

**Correspondence** and requests for materials should be addressed to S.A.S.

**Peer review information** *Nature Communications* thanks Juan Pablo Couso, Xavier Roucou and the other, anonymous, reviewer(s) for their contribution to the peer review of this work.

**Reprints and permission information** is available at <http://www.nature.com/reprints>

**Publisher's note** Springer Nature remains neutral with regard to jurisdictional claims in published maps and institutional affiliations.



**Open Access** This article is licensed under a Creative Commons Attribution 4.0 International License, which permits use, sharing, adaptation, distribution and reproduction in any medium or format, as long as you give appropriate credit to the original author(s) and the source, provide a link to the Creative Commons license, and indicate if changes were made. The images or other third party material in this article are included in the article's Creative Commons license, unless indicated otherwise in a credit line to the material. If material is not included in the article's Creative Commons license and your intended use is not permitted by statutory regulation or exceeds the permitted use, you will need to obtain permission directly from the copyright holder. To view a copy of this license, visit <http://creativecommons.org/licenses/by/4.0/>.

© The Author(s) 2021